The Potential of Machine Learning for a More Responsible Sourcing of Critical Raw Materials

Pedram Ghamisi [ID], *Senior Member, IEEE*, Kasra Rafiezadeh Shahi [ID], Puhong Duan [ID], Behnood Rasti [ID], *Senior Member, IEEE*, Sandra Lorenz [ID], René Booysen, Sam Thiele [ID], Isabel Cecilia Contreras [ID], Moritz Kirsch [ID], and Richard Gloaguen

Abstract—The digitization and automation of the raw material sector is required to attain the targets set by the Paris Agreements and support the sustainable development goals defined by the United Nations. While many aspects of the industry will be affected, most of the technological innovations will require smart imaging sensors. In this review, we assess the relevant recent developments of machine learning for the processing of imaging sensor data. We first describe the main imagers and the acquired data types as well as the platforms on which they can be installed. We briefly describe radiometric and geometric corrections as these procedures have been already described extensively in previous works. We focus on the description of innovative processing workflows and illustrate the most prominent approaches with examples. We also provide a list of available resources, codes, and libraries for researchers at different levels, from students to senior researchers, willing to explore novel methodologies on the challenging topics of raw material extraction, classification, and process automatization.

Index Terms—Deep learning (DL), earth observation, machine learning, mining, raw materials.

I. INTRODUCTION—MINING TOWARD SUSTAINABLE GOALS

THE rapid increase of the human population, the ever-growing levels of economic activity, and the transition toward greener technology are all contributing to an exponential demand in resource extraction and consumption [1]. The transition toward a low-carbon future is paradoxically one of the main drivers to the recrudescence of mining activity. The concept of a purely circular economy where only recyclable material is used, is currently not sustainable due to the increasing demand for metals that were not or used less in the past and the difficulty to recycle more and more complex compounds. Since 2015, more than half of the global material extraction has been originating from mining, with a predicted global extraction of ores to be between two and three gigaton (Gt) by 2050 (see Fig. 1 [1]). The ever-increasing technological innovation
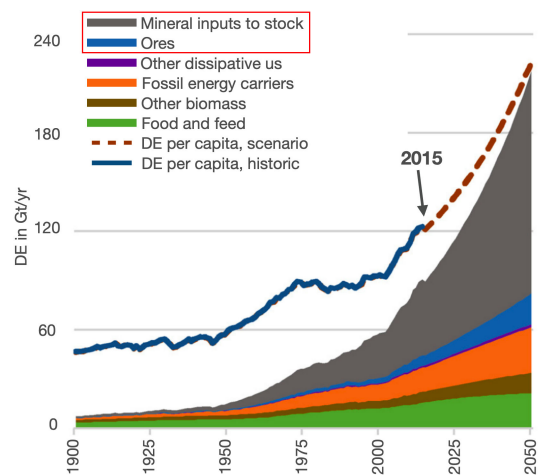
Fig. 1. Global convergence scenario of global material extraction (DE) in Gt/yr by main material groups. The historic trend in DE from 1900 to 2015 is shown in blue and the predicted trend in DE is shown in brown. Mineral inputs to stock and ores contribute to mining [1].

requires a larger variety of elements to improve energy efficiency and miniaturization. The criticality of raw materials has been summarised and categorized by several institutions, such as the European Commission [2] or the Canadian Government [3], and is based on economic importance and supply risk.

There is a growing demand for mineral resources worldwide, and yet the industry is facing increasing obstacles in obtaining public acceptance for new exploration and mining projects. Numerous recent citizen protests highlight the public perception of "destructive" mining projects and increase the reluctance of investors to finance exploration and mine projects [4].

Social scientists attempted to provide a framework to improve the sustainability of metal sourcing. Renn *et al.* [5] provide a framework to establish sustainability objectives.

1) The ecological pillar includes the notions of decarbonization, dematerialization, and rehabilitation of used land (renaturalization).
2) The economic pillar will focus on the circular economy and sustainable welfare.
3) The social pillar considers a fair distribution of risks and benefits, personal, and social opportunities for codetermination of decisions and social well-being, including health.

These three pillars of sustainability can be related to the UN Sustainable Development Goals (SDG) [6]. Not only do we need
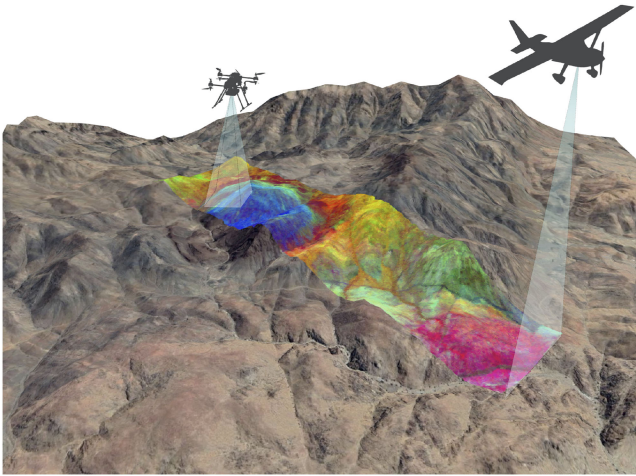
Fig. 2. Airborne platforms with passive sensors represent ideal tools to ensure reliable, safe, and cost-effective monitoring of mining activities.

raw materials to ensure the green deal and the Paris Agreement, but a responsible metal sourcing is required for many of the SDGs.

The responsible sourcing of critical raw materials, thus, requires the development of new technologies both for an improved extraction but also for efficient monitoring. The monitoring of mining activities is fundamental to the respect of environmental, societal, and governance targets. Noninvasive exploration and monitoring techniques can be defined as energy-efficient, safe, and low-impact technologies (see Fig. 2). They assist in the detection and mapping of mineral deposits, improve exploration targeting, and the monitoring of mining activities and their impacts with a minimal environmental footprint while improving social acceptance (e.g., [7]).

The mining industry will embrace the visions of the Industry 4.0 and fully automated mines as well as more technologically sophisticated ore-processing facilities. Better, integrated exploration data have the potential to improve the probability of discovery by reducing and optimizing drilling while boosting information gains. The integration of geological data into multimodal models or digital twins also contributes to optimize drill and blast patterns, create an executable mine plan, and avoid quality issues at the source. Monitoring sensors have also the potential to improve material and equipment flow in an operative mine, to anticipate failures, to enable increased mechanization through automation with real-time updates. At the same time, mining operations often take place in extreme environments and in remote locations. Data processing needs to account for the specific conditions in which remote sensing data have been acquired. Real-time data and the status of machines must be monitored remotely and be modeled with digital twin off-site. All processes will require smart sensors and adapted processing. The monitoring of mining activities will have to deal with big data, smart data processing, and multisensor data fusion.

Imaging sensors are key in the digital evolution of the mining sector. Digitization is used as a catalyst for mines to become more automated by using instruments, networks

and intelligent designs to transition towards "smarter" operations in order to improve forecasting. It includes the forecasting of geological and environmental parameters within which miners work, taking into account the possible dangers. Effective forecasting systems already used by the mining industry include predictive maintenance to take preventive action by collecting data to give priority to repairs via machine use and process parameters. The first aspect of digital processing concerns image enhancement or image preprocessing. Before the evaluation, an image must be improved and optimized for the task at hand. Usually, it concerns all the radiometric and geometric corrections that are required for a proper analysis of the data. There make use of image processing algorithms, such as filters, points, arithmetic, and logical image operations. The result of an image processing is usually an image again. One of the key aspects of preprocessing and focus of recent research concerns denoising. After a potential transformation (e.g., feature extraction and fusion), imaging data are then analyzed to produce evaluations, such as classifications or segmentation.

While many aspects of the digitization and automation of mining operations will, without doubt, increase the efficiency of metal extraction (e.g., [8]), this review will focus on the required imaging sensors and is not intended to cover all the necessary technical developments to achieve Industry 4.0.

The main algorithmic challenges in mining-related applications can be summarized as follows.

1) Complication in acquiring labeled training samples for mineralogical and geological applications. Rocks are fractured, weathered, and altered and composed by a large variety of minerals leading to mineral mixtures at the pixel scale. Defining labels and getting training sets are a challenge.
2) Due to this rock complexity, *in situ*, visual interpretation of extracted samples (e.g., drill-core samples), and accordingly selecting some representative training samples for further analysis (e.g., geochemical analysis) can be subjective and usually based on the experience of a geologist.
3) High-resolution mineralogical laboratory measurements are time-consuming, costly, and require the (partial) destruction of the samples.

These issues have made a simple adaptation of ML techniques developed in other communities extremely challenging for mineral mapping. To partially address these issues, current approaches in the mining community take advantage of mathematical optimization approaches [e.g., sparse, low-rank, and total variation (TV)] and machine/deep learning (DL) methods (e.g., supervised and unsupervised learning) to develop efficient and effective algorithms to provide a clear cutting edge for more responsible sourcing of critical raw materials.

The rest of this article is organized as follows. Section II reviews the imaging technologies, which have largely been utilized for mineral mapping and raw material extraction, at different scales ranging from space-borne remote sensing data to lab-scale measurements, followed by advances in denoising techniques to improve the quality of the acquired data. Sections III and IV are dedicated to advanced machine learning and DL methodologies specifically utilized for mineral mapping. While the first four

sections are mostly on the use of optical data, Section V reviews 3-D point clouds and their challenges in mineral mapping and raw material extraction. Section VI provides a list of available resources and software platforms. Finally, Section VII concludes this article.

II. DATA ACQUISITION, CORRECTION, AND PREPOSSESSING

A. Data Acquisition and Correction

Exploration and mining applications pose special requirements on data quality, originating from both the particulate-related environmental conditions as well as the physical properties of the material to analyze. Targets can vary greatly in scale and feature highly heterogeneous and partly merging classes. Data quality is often influenced by strong topography, dust, unfortunate lighting conditions, and occlusions. These factors challenge proper data acquisition and processing and require innovative approaches in terms of sensor platforms, viewing angles, and data corrections. On top of the challenging environmental conditions, mining applications are demanding in terms of required data quality. Minerals and raw materials are usually characterized by subtle, small-scale changes in observable material properties. In the common example of spectral imaging, the respective features of interest are usually subtle changes in the slope, depth, and position of characteristic spectral absorption features. In the case of mineral identification, not only the composition of the minerals plays an important role but also the mixtures in the mineral assemblages and variations in, for example, grain sizes. Imaging spectrometers can provide an abundance of spectral information spanning from visible to infrared wavelengths. The range of acquisition influences the rock types and minerals that can be accurately identified because of the different behavior of the molecular bonds (e.g., vibrational or electronic absorption processes or stretching and bending). In general, hyperspectral images in the visible to near-infrared (VNIR) and the short-wave infrared (SWIR) provide means to reliably identify alteration minerals, such as oxides or hydroxides, micas, clays, amphiboles, and chlorite. On the contrary, hyperspectral long-wave infrared can be used to map rock-forming minerals, such as feldspars, pyroxenes, and quartz. Depending on the scale of observation, a wide range of platforms, sensors, and processing tools have been developed to tackle these challenges, which will be discussed in more detail in the following sections.

1) Satellite (Space-Borne): Space-borne spectral imaging is a widely employed technique in exploration and mining [9]. A wide range of datasets is available online for free or at low cost, covering large parts of the earth's surface and in addition often providing temporal resolution. On the one hand, the high costs and the effort to transport a sensor into space result in a sensor design that cannot be changed for several years and that does not allow any subsequent customization by the individual user. Alternatively, it enables the establishment of fixed and mature data correction and processing routines. Whereas geometric correction parameters are usually retrievable from the data provider, the influence of topography and atmosphere is compensated with available digital elevation models and established atmospheric correction tools based on atmospheric models and user-defined parameters [10], [11]. To achieve contiguous spectra at acceptable data volumes, developers usually need to make sacrifices regarding spatial sampling to achieve sufficient spectral resolution, resulting in large ground sampling distances of most space-borne hyperspectral sensors, e.g., EO-1 Hyperion sensor (30 m, out of operation today) or the recently launched PRISMA (30 m). Developers of new space-borne sensors face crucial challenges, such as low signal-to-noise ratio values due to the extreme influence of the atmosphere, high sensor costs, and time-consuming processing of the retrieved, large datasets [12].

2) Crewed Aircraft (Airborne): In the last decades, airborne surveys have been the most common way to acquire high-quality remote sensing data, which has led to a strong development in acquisition workflows and correction tools [13], [14]. The reasons for their popularity are manifold: The variety of deployable sensors is nearly unlimited, and the spatial resolution and coverage are reasonable for a wide range of applications and can be adjusted by changing the flight altitude to fit the individual objective. However, extensive flight campaigns are usually costly, weather dependent, and require a not negligible amount of infrastructure and logistics. Multitemporal measurements are accordingly time- and cost-consuming and sources for failures are manifold. In contrast to satellite surveys, prior knowledge of the approximate position of the target is crucial. At common flight altitudes (several hundred meters to kilometers), a radiometric correction with ground reference targets is not applicable and the geometric correction is complex due to the movements of the platform. Properly corrected airborne datasets can feature a high spatial and spectral resolution and coverage with significantly reduced noise in comparison to space-borne data, not at least due to the possibility to fly any sensor regardless of its weight. However, the costliness often denies small-budget stakeholders from targeted airborne surveys.

3) Uncrewed Aircraft (Drone-Borne): Uncrewed aerial systems (UASs), also referred to as drones, recently became a major developing branch in the field of autonomous vehicles. Lightweight, low-cost, customizable, and usable by anyone and nearly anywhere, UAS offers individual solutions for a wide range of applications. Imaging sensors are a common UAS payload and can range from standard RGB frame or video cameras up to multi and hyperspectral imaging sensors, which allow the mapping of chemical and physical properties of the observed target. Current developments in UAS technology look to increase flight times, payload, and ease of operation, and artificial intelligence (AI) has a key role in this goal [15], [16]. Parallel to the technical development, the number of prospective users and application fields for drone-borne mapping rises fast, including mineral exploration, mining, and environmental monitoring due to, for example, the possibility of acquiring data with high spatial resolution covering extensive regions and even reaching complicated terrains. Drone platforms also create new challenges due to complex geometric and radiometric conditions, as well as data acquisition, quality, integration, and interpretation [17]. Adequate data corrections and interpretation require advanced tools and the development of adapted methodology for geometric referencing and data fusion [18]. Autonomous flying and drone
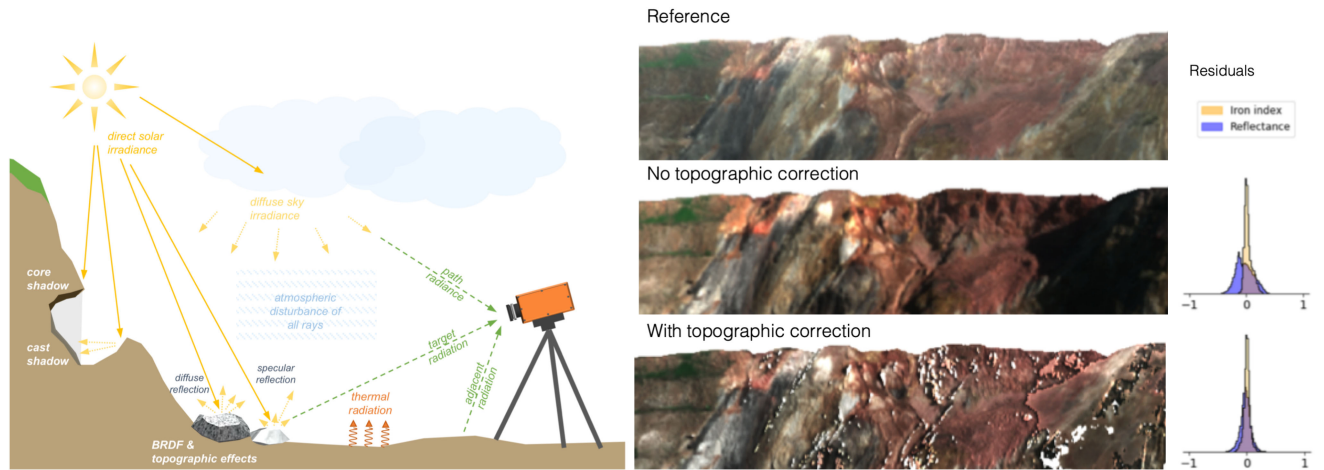
Fig. 3. Left: Paths of radiance and external radiometric disturbances in a hyperspectral field acquisition [23], [24]. Right: Importance of topographic corrections for the retrieval of reliable reflectance data [25].

swarms have been made possible for mono- or nonsensoric applications such as transport, delivery, and large photogrammetric surveys [19]. Real-time flight planning adjustments, the complex preprocessing of imaging data, multimodal/high-dimensional data support as well as heterogeneous fleet management remain challenging and require further research.

4) Terrestrial/Small-Angle Scans: Geological targets, such as cliffs, vertical outcrops, or mine faces, tend to be hardly observable by common nadir or near-nadir imagery. This raised the need for a new approach of hyperspectral data acquisition at small angles. Usually, this is achieved by horizontal or slightly tilted sensor mounting on a tripod or rotary stage (in case of a push broom sensor) [20]–[22], alternatively, any other sensor-bearing platform, such as a car, boat, or low-altitude UAS, can be used. Even if the acquisition is straightforward and requires no additional platform, the radiometric and geometric correction of the data is extremely complex (see Fig. 3). The main disturbances originate from strong topography-induced illumination differences, shadows, and in the case of high-distance measurements, atmospheric effects. Orthorectification, visualization, and integration involve a lot of intricate processing steps. Recent developments utilize direct 2.5-D/3-D representations of the acquired data to overcome these challenges. A more detailed review can be found in Section VI.

5) Lab-Scale: Hyperspectral imaging at lab-scale or near-field (spatial sampling distances in the millimetre to the sub-millimetre range) is a highly demanded topic in not only the exploration, mining, and processing industry, but also in the framework of most remote sensing studies regarding validation and detailed sample analysis. The need for near-field hyper-spectral imaging data acquisition, processing, and interpretation arises from the fact that hyperspectral imaging lab setups provide means to rapidly scan large amounts of data with high-spectral resolution and coherent coverage in a noninvasive and nonde-structive manner. Spectral imaging of rock material in mining and processing is usually highly automated and simplified to produce only a few classification criteria, for example, to decide between waste rock and ore or between different ore grades.

Since the focus lies on high throughput, the employed sensors need to be adequately highly specialized, robust, and reduced to the essential task. In exploration and lithological mapping, the amount and complexity of mineral phases to be distinguished is usually much higher, and simple indices are no longer sufficient. Instead, the acquisition and careful analysis of full spectra is required. Moreover, depending on the size of the project, large quantities of samples still have to be analyzed. The upscaling of locally constrained geochemical data, multisensor data fusion, and real-time processing are the most urgent challenges of this scale.

B. Denoising

Recent advances in remote sensing technologies provide non-invasive techniques for mineral exploration and mining monitoring. On the other hand, different technologies contain different noise and artifacts that need to be reduced to guarantee reliable results in the whole processing chain. For instance, optical remote sensing data contain mixed noises, such as sparse, stripping, Gaussian, and Poisson noise. As a result, noise reduction can be considered as a preprocessing step that can boost mineral exploration and mining [26]–[29].

1) State of the Art: Remote sensing images are often degraded by two major sources, i.e., the imaging systems and instrumental noises as well as the atmospheric effect that has been discussed in the previous section. The instrumental noises include thermal, quantization, and shot noise often modeled with the Gaussian distribution. The missing pixels, lines, and stripes (often exist in push-broom imaging systems) can be modeled as the sparse noise with the Laplace distribution [30]–[32]. Therefore, we assume

$$\mathbf{H} = \mathbf{X} + \mathbf{S} + \mathbf{N} \tag{1}$$

where $\mathbf{H}$ is the observed image, $\mathbf{S}$ is the independent additive sparse noise, and $\mathbf{N}$ is the additive Gaussian noise. Therefore,

$\mathbf{X}$ can be estimated using an optimization problem given by

$$\hat{\mathbf{X}} = \arg \min_{\mathbf{X}} Q(\mathbf{H}, \mathbf{X}) + \lambda R(\mathbf{X}) \tag{2}$$

where functions Q and R, respectively, define the fidelity and the penalty terms balanced by the tuning parameter λ. Depending on the application and the noise model, problem (2) can be subjected to equality and inequality constraints.

Signal and image denoising have been considerably improved over the past decades. The emergence of wavelets made a significant impact on the field of denoising compared to the Fourier transform and conventional filtering techniques, such as mean or median filtering [33]. Wavelet transforms decompose a signal into different scales (resolutions) assigned by frequency ranges, and therefore, the noise can be successfully decorrelated from the signal. This type of representation using wavelets was the beginning of the sparse and redundant representations that have shown great advantages in many applications particularly in denoising [34]. In sparsity theory, signals are spanned by overcomplete dictionaries, and therefore, they can be reconstructed using a few representative dictionary atoms [35]. Later on, sparse and low-rank representations showed considerable advantages compared with the sparse and redundant representations [36]–[38]. For instance, Rasti *et al.* [36] showed that for hyperspectral images, low-rank models outperform the sparse models due to the spectral redundancy [36]. Therefore, sparse and low-rank techniques have shown to be a great advantage in hyperspectral image denoising [39], [40]. An automatic hyperspectral restoration technique, entitled HyRes, was proposed in [41], which is based on the following cost function:

$$\hat{\mathbf{W}} = \arg \min_{\mathbf{W}} \frac{1}{2} \left\| \mathbf{H} - \mathbf{DWV}^T \right\|_F^2 + \sum_{i=1}^{r} \lambda_i \left\| \mathbf{w}_{(i)} \right\|_1 \tag{3}$$

where $\mathbf{D}$ and $\mathbf{W}$ are the wavelet basis and coefficients, respectively. $\mathbf{V}$ is given by the singular value decomposition (SVD): $\text{SVD}(\mathbf{H}) = \tilde{\mathbf{U}}\tilde{\mathbf{S}}\mathbf{V}^T$ where the subspace bases (i.e., the columns of $\mathbf{V}$) were selected using the hyperspectral Stein's unbiased risk estimator [42]. Similar to HyRes, fast hyperspectral denoising (FastHyDe) [43] also uses a low-rank technique that first projects the HSI into a subspace and, then, uses BM3D [44] for spatial denoising. Noise-adjusted image recovery using low-rank matrix approximation (NAIRLMA), proposed in [45], uses a combination of a low-rank norm and a sparsity norm. Hyperspectral denoising via robust principal component analysis (RPCA) and self-similarity was proposed in [46] for mineral mapping, which applies the block-matching and three-dimensional collaborative filtering (BM3D) [44] to the components extracted by the RPCA [38].

TV denoising [47] is another efficient denoising approach, which minimizes the signal variations using

$$\hat{\mathbf{X}} = \arg \min_{\mathbf{X}} \frac{1}{2} \left\| \mathbf{H} - \mathbf{X} \right\|_F^2 + \lambda \text{TV}(\mathbf{X}) \tag{4}$$

where TV is the total variation function. So many variations of (isotropic and anisotropic) TV denoising have been adapted for different images considering the characteristics of the observed signal. For instance, the spatio-spectral TV proposed in [48] exploits anisotropic spatial-spectral TV penalties for hyperspectral
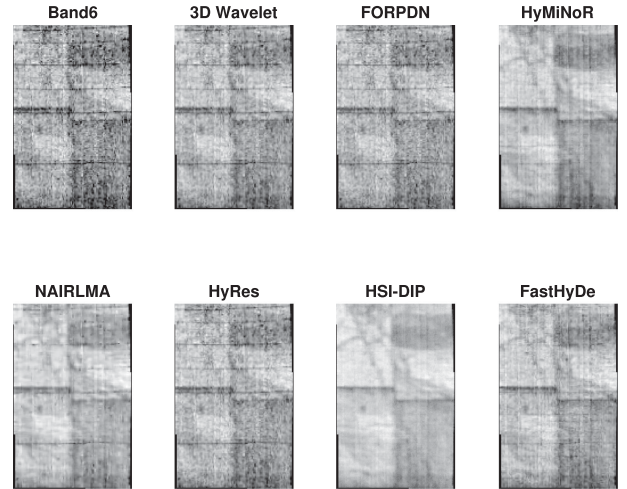

Fig. 4. Results of applying different denoising methods to the hyperspectral dataset captured by using FX10 sensor from drill-core samples.

denoising to capture the spectral and spatial correlations. Rasti *et al.* proposed hyperspectral mixed noise reduction (HyMiNoR) in [49], which exploits the spectral gradient to capture the spectral correlation. The low-rank TV was also proposed for both feature extraction and denoising [36], [50].

DL-based denoising techniques are considered state-of-the-art in the signal and image processing community. DL-based denoising techniques designed for RGB images can often be used for remote sensing image denoising, however, they cannot take into account the specific characteristics such as spectral dependency. Additionally, the main challenge to use DL-based methods is the absence of a comprehensive training database for different remote sensing applications such as mining. Therefore, training the supervised networks is cumbersome. On the other hand, unsupervised deep networks use the observed image and iteratively train the network such as deep image prior (DIP) [51]. In DIP, the observed image is used to train an unsupervised convolutional encoder–decoder for generating the noiseless image from noise. Noise2Noise [52] uses noisy image pairs as targets and inputs for training the network and Noise2Void uses the noisy image as the target and input, however, it exploits a blind-spot network to preserve learning the identity. A convolutional neural network (CNN) using a blind-spot network then predicts a pixel using all the neighboring pixels except itself.

2) Experimental Results: Here, we show how denoising techniques can be applied as the final step of the preprocessing chain to boost mineral exploration. Fig. 4 compares different denoising techniques applied to hyperspectral dataset captured by the FX10 sensor (400–1000 nm) from four sections of drill-core samples (see [26] for details). The comparison reveals that the low-rank techniques (i.e., HyRes, FastHyDe, HyMiNoR, and NAIRLMA) outperform the full-rank ones (i.e., 3-D Wavelets and FORPDN). The DL-based technique, HSI-DIP, visually outperforms the other techniques. The positive effect of denoising techniques over the data is evident. This improvement allows more reliable identification of different patterns observed in the data, such as lineaments which in this case, relate to mineral

veins. This can have a great influence when mapping minerals and, therefore, boost mineral exploration since different veins and their composition can indicate, for example, different alteration zones in a geological deposit.

III. ADVANCES IN CLASSIFICATION APPROACHES

Recent advances in remote sensing techniques (e.g., hyperspectral imaging) assure the fast and reliable acquisition of geological information in a sustainable manner. In order to analyze the remote sensing data, various machine/DL approaches (i.e., supervised and unsupervised) have been developed [53]. Among those, supervised learning approaches rely on labeled samples (also known as training samples), which, in most remote sensing applications, are hard to acquire [54]. This is the same for geological applications where training data or ground truthing is not always available. Unsupervised learning (also known as clustering) approaches have received significant attention due to their empirical success, and also, their capability of analyzing remotely sensed data without a need for training samples or any prior knowledge [55], [56]. Therefore, clustering can provide valuable insight into the under process remote sensing data for mineral exploration.

A. Unsupervised Approaches

Clustering has become a mature research field. Many studies have been devoted to developing spectral, spatial, and spectral–spatial clustering approaches for remote sensing data analysis [57]–[59]. In general, clustering approaches can be divided into the following two main categories: 1) conventional shallow clustering approaches and 2) DL-based clustering approaches.

1) Conventional Shallow Clustering Approaches: K-means clustering is one of the most well-known clustering approaches [56], [60]. K-means is regarded as an iterative process, where the algorithm initially selects random cluster centroids; then, it computes the distance (i.e., Euclidean distance) between data points and the selected centroids, consequently, data points closer to a cluster centroid are assigned to that cluster. The process of refining the centroids selection is carried on until, either the maximum number of iterations reaches or the cluster centroids do not change further [60]. However, centroid-based clustering approaches are efficient when the dataset has a low complexity; while, in many studies, like remote sensing datasets (specially hyperspectral images), the spectral variability can cause poor performances of such approaches [58]. Therefore, more advanced clustering approaches have been proposed in recent years, to name a few, density-based clustering approaches, graph-based clustering approaches, and subspace-based clustering approaches [56], [61]. Among the aforementioned clustering approaches, subspace-based clustering approaches have drawn considerable attention in remote sensing studies [55], [57]–[59], [61].

Sparse subspace-based clustering (SSC), is a well-known subspace-based approach [61], benefits from the so-called *self-expressiveness* property [58]. In short, *self-expressiveness* property expresses that each data point can be written as a linear combination of other data points from the same subspace.

In other words, if two data points are from the same subspace, in the sparse representation, their relation is identified by a nonzero coefficient; otherwise, zero in the representation shows that two data points are not from the same subspace. The sparse coefficient matrix is computed as follows:

$$\arg \min_{\mathbf{C}} ||\mathbf{C}||_1 + ||\mathbf{X} - \mathbf{X}\mathbf{C}||_F^2 \qquad (5)$$

where $\mathbf{C} \in \mathbb{R}^{N \times N}$ represents the sparse coefficient matrix of the original image ($\mathbf{X}$). To generate the final cluster map, SSC computes the similarity matrix as $\mathbf{W} = |\mathbf{C}| + |\mathbf{C}^T|$, and then, feeds $\mathbf{W}$ to spectral clustering for the final step [61]. Although SSC usually outperforms traditional clustering approaches in terms of accuracies, its concept suffers from a few shortcomings. One shortcoming is that SSC uses all data points to compute the sparse representation; such a strategy is, therefore, computationally and temporally expensive [55], [59], [62]. As a result, SSC fails in handling large-scale datasets. Thus, various studies focus on using a subset of the original dataset for sparse representation computation. For instance, in [55], the authors proposed a scalable exemplar-based subspace clustering approach (the so-called ESC). In ESC, sparse coefficient matrix is constructed by using a subset of representative samples (also known as exemplars) from $\mathbf{X}$. In addition, You *et al.* [55] designed a search function to identify the exemplars by minimizing a maximum representation cost of $\mathbf{X}$. One can rewrite (5) as

$$\arg \min_{\mathbf{C}} ||\mathbf{C}||_1 + ||\mathbf{X} - \mathcal{X}_0 \mathbf{C}||_F^2 \qquad (6)$$

where $\mathcal{X}_0 \in \mathbb{R}^{N \times P}$ is a subset of representative samples. P expresses the number of representative samples. Therefore, spectral clustering cannot be directly applied to $\mathbf{W}$. To cope with the problem, for each $\mathbf{c}_i$, which is the ith column vector in $\mathbf{C}$, t nearest neighbors with the largest positive inner products are found. Then, the produced $\mathbf{W}$ is passed through spectral clustering to generate the final cluster map.

2) DL-Based Clustering Approaches: Autoencoders (AEs) are the most representative DL-based clustering techniques [63], which aim to reconstruct the original image ($\mathbf{X}$) in two phases (i.e., encoder and decoder). In the encoder phase, discriminant features (also known as latent features) are extracted, and then, the latent features are employed to shape the reconstructed image ($\mathbf{X}'$). Thus, the main aim in an AE-based network is to minimize the loss ($\mathcal{L}$) between $\mathbf{X}$ and $\mathbf{X}'$ often computed using the mean square error

$$\mathcal{L} = \frac{1}{N} \sum_{i=1}^{N} ||\mathbf{x}_i - \mathbf{x}'_i||_2^2 \qquad (7)$$

where $\mathbf{x}_i$ and $\mathbf{x}'_i$ are the ith column vectors of $\mathbf{X}$ and $\mathbf{X}'$, respectively. At last, the trained network produces informative features that can be clustered by a clustering approach. Such approaches are robust against the spectral variability within the data points in a hyperspectral image, and offer an end-to-end block paradigm to process high-dimensional datasets [63].

3) Clustering Approaches in Mineralogical and Geological Applications: Clustering approaches have been deployed intensively for mineralogical and geological applications [59],

TABLE I
QUANTITATIVE ASSESSMENT OF ALL CONSIDERED CLUSTERING APPROACHES

Classes	Test	Different clustering approaches					
		K-means	FCM	LSC	ESC	HESSC	AE
Clay	1062	35.70	36.70	53.08	17.80	**55.98**	52.60
Glimmerite-Carbonatite	791	0.00	0.00	4.79	27.75	**61.59**	29.74
Glimmerite	1048	41.93	45.53	70.37	4.00	0.36	62.97
Dark-rocks	994	66.12	64.78	69.16	21.43	34.46	**95.71**
Dust	964	60.55	62.38	**73.78**	66.67	0.00	62.56
Feldspar-vein	1061	46.52	46.15	0.00	5.71	**91.61**	70.70
Fenite	1065	46.48	44.54	**63.22**	40.77	62.16	42.42
Water	1011	35.29	35.31	33.83	99.12	63.42	**100.00**
OA		44.36	44.77	45.89	31.57	48.43	**62.67**
AA		41.57	41.92	46.03	35.41	46.20	**64.59**
Kappa		0.36	0.37	0.38	0.21	0.41	**0.57**

[64]–[68]. For instance, Guo *et al.* [64] proposed a 1-D spatial domaining approach that segments drill-core hyperspectral images into meaningful domains along with the depth. Similarly, in [66], the usability of SSC approaches for drill-core hyperspectral domaining has been evaluated, in which according to the authors' observations, incorporating spatial information with spectral information considerably improves the final domaining results. Fouedjio *et al.* [65] investigated the usability of geostatistical clustering approaches to domain an iron ore deposit located in Western Australia. Domaining of drill-core hyperspectral images can provide valuable but general mineralogical information [59]. Additionally, domaining techniques are computationally affordable for drill-core; however, these techniques are hard to apply on large-scale datasets (e.g., UAV-based data). To cope with the aforementioned challenges, and produce a detailed mineral cluster map, fast and scalable clustering approaches are required.

In [59], the authors proposed a fast and automatic hierarchical sparse subspace-based clustering approach (HESSC). HESSC was designed to process large-scale datasets, and its performance was tested on drill-core hyperspectral images. The experimental results showed its superiority compared to other clustering algorithms; however, HESSC only utilizes spectral information in the analysis procedure. In [67], authors proposed a multisensor sparse-based clustering approach (Multi-SSC) for multisensor data fusion. Multi-SSC inherits a similar structure as HESSC; whereas, it incorporates spatial information, which is derived from a high spatial-resolution image. Utilizing such complementary information allows Multi-SSC to preserve spatial structures. The performance of Multi-SSC was evaluated for the application of UAV-based geological mapping, where Multi-SSC was capable of distinguishing mineralogical and geological targets, accurately, compared to the state-of-the-art clustering approaches.

4) Experimental Results: In this section, the performances of different machine/DL (i.e., supervised and unsupervised) approaches are examined. A mineral dataset, i.e., Finland (see Fig. 5), is adopted for the quantitative and qualitative assessment of different approaches. The Finland dataset was captured by a 0.6 Mp Rikola hyperspectral imagery. This image contains 50 channels ranging from 0.5 to 0.9 μm, and its spatial resolution
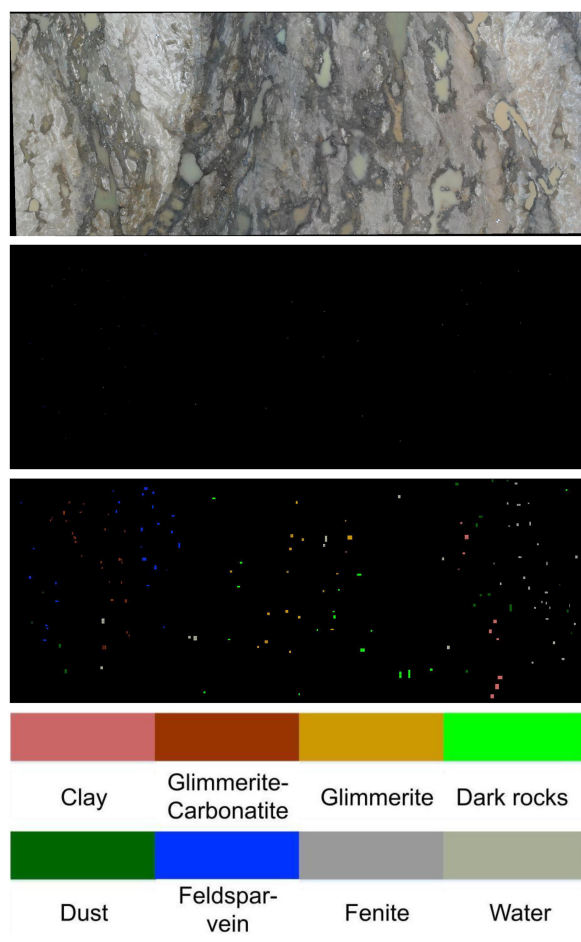

Fig. 5. Finland dataset. From top to bottom: RGB image, training samples, testing samples, and class name.

is 3.3 cm. The RGB dataset was obtained by a senseFly RGB camera. Its spatial resolution is 1.5 cm. Both of them have been registered before the fusion operation. They have 717×1848 pixels. The experimental results using unsupervised learning approaches, can be found in Table I and Fig. 6; furthermore, the experimental results using supervised and multisensor data fusion approaches are presented in Fig. 8 and Table II.
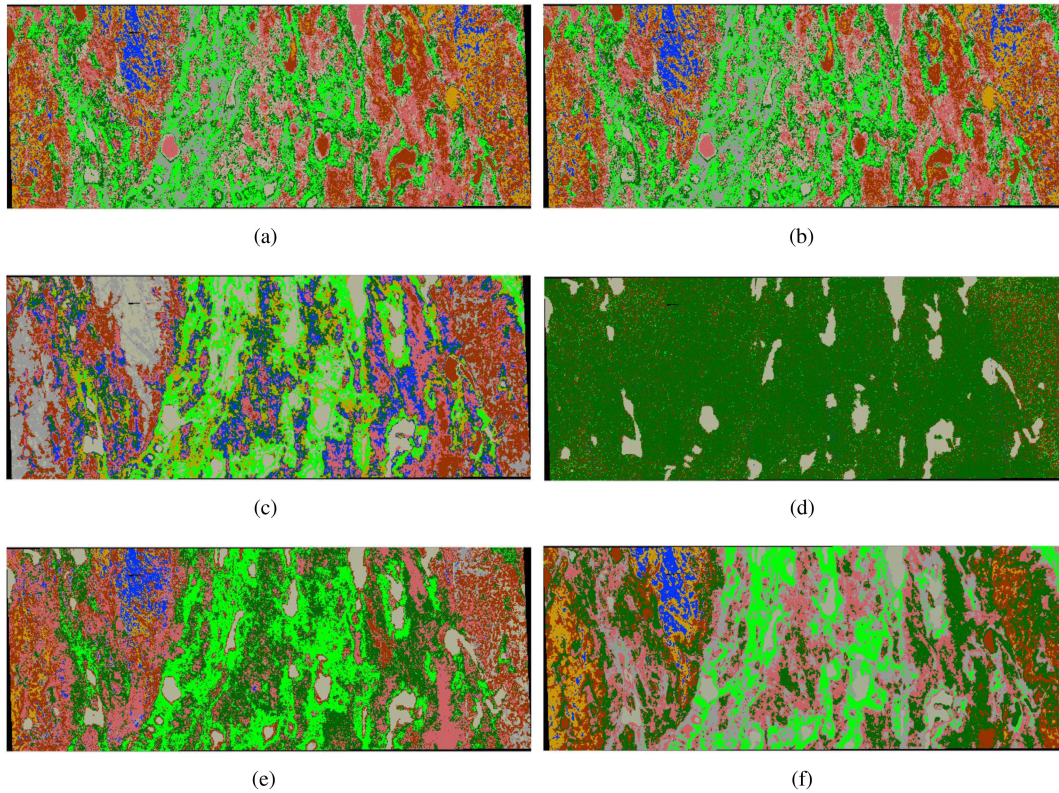
Fig. 6. Cluster maps obtained by different approaches as, (a) K-means, (b) FCM, (c) LSC, (d) ESC, (e) HESSC, (f) AE.

TABLE II
CLASSIFICATION ACCURACIES OF ALL CONSIDERED APPROACHES

Classes	Train	Test	Different classification approaches						
			SVM_{HSI}	SVM_{RGB}	FDSI	CNN	CNMF	IIDF	SubFus
Clay	12	1050	75.86	77.91	**100.0**	88.99	70.92	74.63	96.10
Glimmerite-Carbonatite	42	749	30.53	19.70	34.02	88.28	75.57	35.65	**98.93**
Glimmerite	16	1032	92.11	76.56	**100.0**	90.84	65.08	90.41	87.50
Dark-rocks	12	982	83.72	78.67	**95.20**	91.83	67.81	82.67	67.41
Dust	28	936	55.23	53.18	63.35	84.30	78.72	61.21	**93.91**
Feldspar-vein	20	1041	86.63	0.00	**100.0**	99.56	37.23	89.56	89.82
Fenite	12	1053	79.19	0.00	**100.0**	98.45	33.02	95.96	94.68
Water	16	995	**100.0**	72.81	**100.0**	**100.0**	85.16	**100.0**	86.03
OA			65.95	49.89	74.79	**92.80**	63.38	71.42	89.08
AA			75.41	47.35	86.57	**92.78**	64.19	78.76	89.30
Kappa			61.34	43.42	71.39	**91.77**	58.42	67.49	87.51

In this study, we evaluate the performance of two conventional clustering algorithms (i.e., K-means [60] and fuzzy c-means (FCM) [69]); three scalable sparse-based clustering approaches (i.e., landmark-based spectral clustering using sparse representation (LSC) [70], ESC [55], and HESSC [59]); and one DL-based clustering approach (i.e., AE [54]). In the AE-based clustering approach, the extracted latent features from AE are passed through K-means to generate the clustering results. Moreover, to further promote employing advanced clustering approaches in the field of mineralogy and geology, we provide a list of online available clustering toolboxes in Section VI.

Fig. 6 illustrates the clustering maps of the unsupervised classification approaches. The qualitative comparison of the clustering maps reveals that AE [see Fig. 6(f)] produces less "noisy" clusters.

Additionally, to quantitatively assess the performance of studied clustering approaches, the following evaluation metrics are used: overall accuracy (OA), average accuracy (AA), and kappa coefficient (Kappa). According to the obtained quantitative results (see Table I), several conclusions can be made. Two conventional clustering approaches (i.e., K-means and FCM) have similar and weak performances compared to other studied approaches.

The results confirm that HESSC performs well compared to other studied clustering approaches. However, HESSC considers the structure lying between data points as linear, while
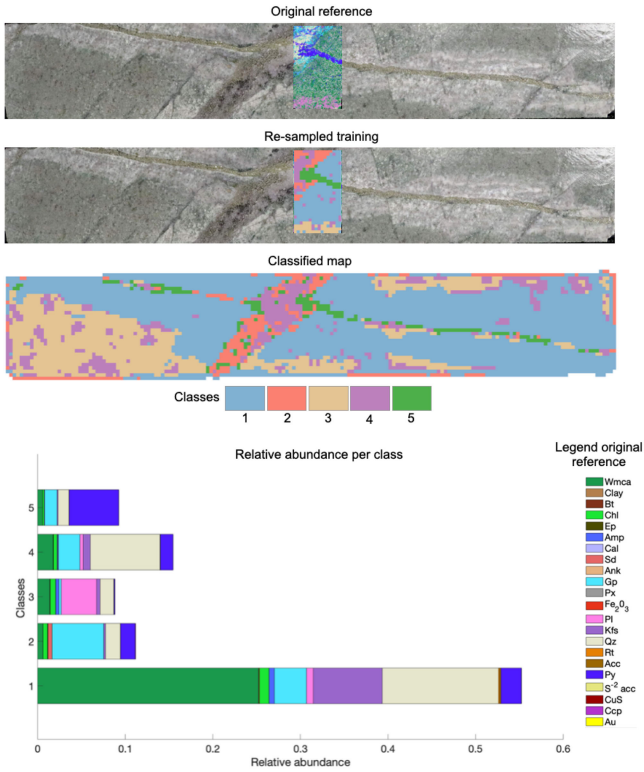
Fig. 7. Classification map of a drill-core sample obtained by training an RF classifier using VNIR-SWIR hyperspectral data acquired with a FENIX sensor and high resolution mineralogical data [75]. Classification accuracies are of 74%.

in real-world high-dimensional datasets, there exists nonlinear relation between data points [71]. On the other hand, AE obtains the highest clustering accuracy among all studied clustering approaches. This indicates the capability of DL-based clustering algorithms to capture nonlinear intrinsic structures between data points and their suitability for mineralogical and geological applications.

B. Supervised Approaches

Traditional methods to map rocks and minerals with hyperspectral data mainly focus on the visual interpretation of the sample spectra and a comparison with reference spectral libraries, e.g., USGS Spectral Library [72]. Endmember spectra obtained with, e.g., Pixel Purity Index, NFINDR, and vertex component analysis have been used to derive the main spectrally distinct minerals [73]. The spectral angle mapper has also been widely used to select the best match for unknown pixels according to the reference spectra or the retrieve endmembers [74]. These methods, which are based on intensive expert interaction, have shown satisfactory performances but they are subjective, time-consuming, and rely on extensive expertise. Recent developments in the processing of hyperspectral data for mineral exploration make use of available datasets routinely acquired during exploration campaigns. Examples of these are whole-rock geochemistry or high-resolution mineralogical analysis providing identification and quantification of minerals. Such information can be used as a reference to generate training and test

datasets [75], [76] as can be seen in Fig. 7. Here, hyperspectral and scanning-electron microscopy mineral liberation analysis (SEM-MLA) data from a drill-core sample of a porphyry deposit are fused. The hyperspectral data have a spatial resolution of 1.5 mm/pixel and 450 bands covering the VNIR and SWIR (from 380 to 2500 nm). SEM-MLA provides high-resolution mineralogical data. These were coregistered and resampled to the resolution of the hyperspectral data to be able to upscale the detailed mineralogical composition. This, therefore, permits the use of robust supervised machine learning approaches to accurately identify and map the distribution of different minerals (see Fig. 7).

Outside the mineral exploration community, a huge number of complex algorithms have been recently developed in the fields of machine/DL, computer vision, and image and signal processing. Most of those approaches take advantage of—and at the same time, they require—the increasing power of advanced computing. Inspired by these advancements, machine (deep) learning techniques have been utilized for a variety of applications for mineral mapping (classification) and characterization. These classifiers, in a similar manner to unsupervised approaches mentioned in the previous section, can be broadly split into the following two categories: 1) Conventional shallow classifiers and 2) DL-based classifiers. In the following, we will describe each of these categories in more detail. We also describe one representative from each of these categories whose superior performance has been validated for mineral mapping.

1) Conventional Shallow Classifiers: Currently, various spectral classifiers have been investigated for classification of remote sensing images [77], such as support vector machine (SVM) [78], random forest (RF) [79], and multinomial logistic regression [80]. Here, we briefly describe a very popular spectral classifier, i.e., SVM, because of its strong ability in tackling high-dimensional data with a limited number of training samples, which makes this classifier well-suited for a variety of mineralogical applications.

SVM aims at defining an optimal hyperplane to separate different classes of interest in a multidimensional feature space. The best hyperplane is the one that makes the maximum margin between different classes, which is obtained by solving an optimization objective function. Specifically, let $\mathbf{X} = \{\mathbf{x}_i\}$, $\mathbf{X} \in R^{M \times N_t}$ denote the test set, where M indicates the feature dimension of each test sample and N_t represents the total amount of test samples. The class label is named as $\mathbf{Y} = \{y_i\}$, $\mathbf{Y} \in R^{N_t}$, where y_i stands for the label of ith test sample x_i. $\mathbf{Z} = \{\mathbf{z}_n\}$, $n = 1, 2, \ldots, N_{\mathrm{tr}}$ is the training set, in which the label of each training sample $\mathbf{z}_n$ is defined as y_n. The SVM classifier is expressed as

$$f(\mathbf{x}_i) = \mathrm{sign}\left(\sum_{n=1}^{N_{\mathrm{tr}}} \lambda_n y_n \Phi(\mathbf{x}_i, \mathbf{z}_n) + b \right) \qquad (8)$$

where λ_n denotes the Lagrange multiplier, y_n is the label of $\mathbf{x}_i$ sample, and b is the bias. $\Phi(\mathbf{x}_i, \mathbf{z}_n)$ represents a linear or nonlinear kernel function. For the hyperspectral image classification task, the Gaussian radial basis function kernel has been widely used since the kernel can well tackle complex, nonlinear
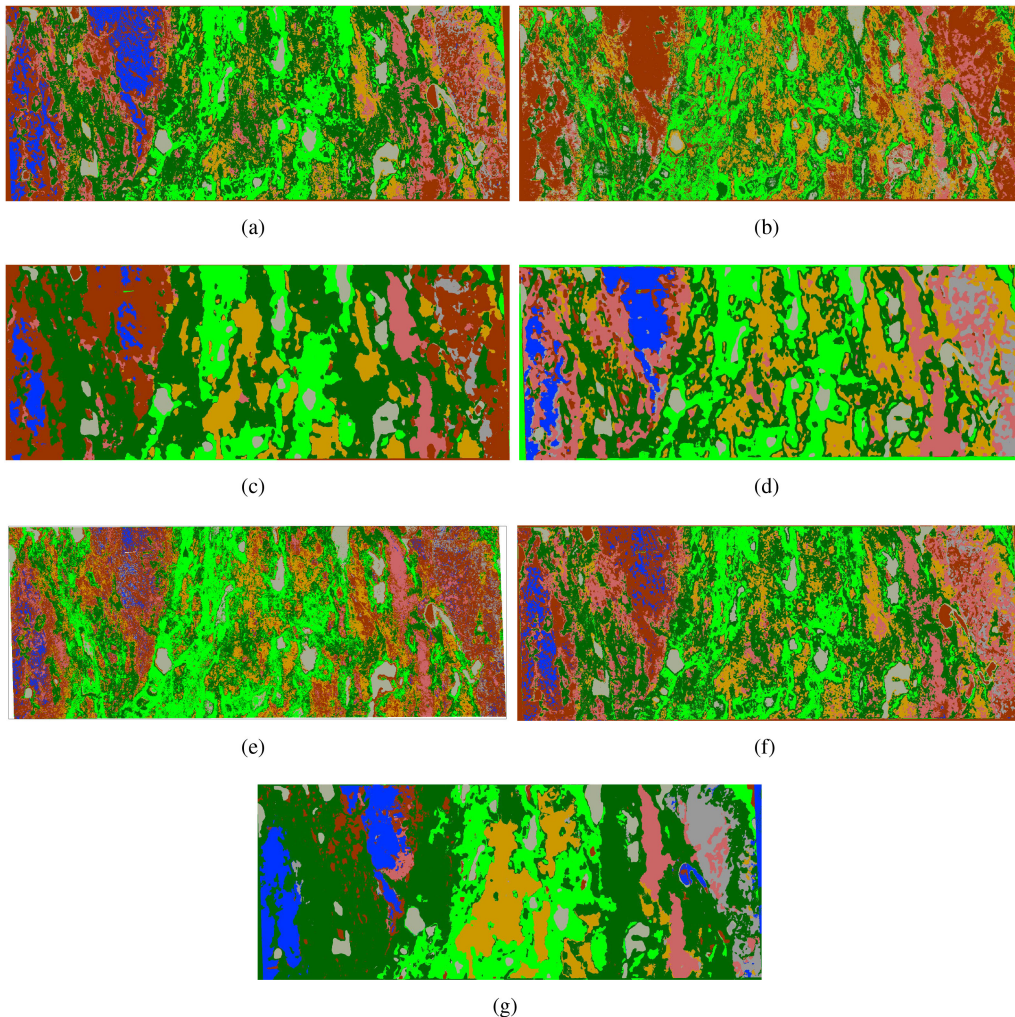
Fig. 8. Classification maps of different approaches. (a) SVM on hperspectral data. (b) SVM on RGB image. (c) FDSI on HSI data. (d) CNN on hyperspectral data. (e) CNMF. (f) IIDF. (g) SubFus.

high-dimensional data. For a detailed solution of (8), we refer readers to [81].

Most recently, in [82], the performance of several conventional (e.g., PCA [83] and MNF [84]) and recent shallow feature extraction approaches, e.g., orthogonal total variation component analysis (OTVCA) [85] and wavelet-based sparse reduced-rank regression (WSRRR) [86])) have been evaluated on three case studies from geological hyperspectral mapping campaigns, including drone-borne mineral exploration, terrestrial paleoseismic outcrop scanning, and thermal hyperspectral lithological mapping with sparse or partly inaccurate validation data. The outcome of the study reveals the advantages of innovative feature extraction algorithms in terms of classification accuracy and geological interpretability.

2) DL-Based Classifiers: DL, as a subfield of machine learning, aims for automatizing the main building blocks of the machine learning approaches (i.e., feature extraction and classification) by developing an end-to-end framework. DL classifiers automatically receive the input, performs automatic feature extraction and classification by considering the unique nature of the input data (instead of those hand-crafted feature extraction designs in machine learning), and output classification maps. With an adequate amount of training data, DL approaches can outperform any other shallow machine learning approaches in terms of mapping quality [54]. Among deep neural networks, CNNs are the most widely used deep classifiers whose success has been validated in mining-related applications [87]. We briefly describe a simple CNN [54] for the task of classification, which mainly consists of three components, i.e., convolutional layers, pooling layers, and fully connected layers. The deep features can be obtained by convolution operation, which can be expressed as

$$\mathbf{y}_j = \sum_{i=1}^{d} f(\mathbf{x}_i * \mathbf{w}_j + b_j), j = 1, 2, \ldots, k \qquad (9)$$

where k denotes the number of filters in the convolutional layer, $\mathbf{w}_j$ and b_j indicate the weight and bias of the jth filter, $\mathbf{x}_i$ is the ith feature map of the input $\mathbf{X}$, d is the amount of spectral channels, $*$ is the convolution operation, and $f(\cdot)$ is the activation function.

A widely used activation function, i.e., ReLU, is adopted in this work, which can be formulated as

$$\sigma(\mathbf{x}) = \max(0, \mathbf{x}). \tag{10}$$

Then, the extracted features are further processed with the pooling layer to decrease the size of feature maps. Specifically, an average pooling operation is performed on the feature maps

$$z = \frac{1}{N} \sum_{(i,j) \in \Delta} \mathbf{x}_{ij} \tag{11}$$

where N denotes the number of elements in local region Δ. x_{ij} is the element at the position (i, j).

Finally, the fully connected layers are adopted to extract high-level features and output the final results, which can be expressed as

$$\mathbf{Y} = \sum_i f(\mathbf{W}\mathbf{X}^T + \mathbf{b}) \tag{12}$$

where $\mathbf{Y}, \mathbf{W}, \mathbf{X},$ and $\mathbf{b}$ are the output, weight, input, and bias of a fully connected layer, respectively.

3) Experimental Results: To evaluate the classification performance of different approaches, three representative classification methods are adopted, including SVM classifier [88], fusion of dual spatial information (FDSI) [89] and CNN [54]. All parameters of these methods are set according to the corresponding publications. Experiments are performed on the Finland dataset, which is described in Section III-A4.

The visual classification results are shown in Fig. 8. As shown in Fig. 8, the SVM classifier produces "noisy" labels [see Fig. 8(a), (b), and (e)]. This is because the spatial information between adjacent pixels is not taken into consideration. By contrast, other spectral–spatial classification methods such as FDSI and CNN can better preserve the homogeneous areas belonging to the same mineral. Furthermore, Table II lists the objective indexes of different approaches. The SVM classifier performed on hyperspectral data yields higher classification accuracies than that of the RGB image, which also confirms that the rich spectral information of hyperspectral data is essential for mineral mapping. The FDSI method performs well on six classes. However, the classification accuracy of the second class (Glimmerite–Carbonatite) is relatively low because the discrimination between the Glimmerite–Carbonatite and Glimmerite classes is small. The CNN-based classification method can achieve better classification performance than the FDSI method, since the DL-based method can extract more discriminative information ranging from shallow-level to high-level spatial features.

IV. FROM A SINGLE SENSOR TO MULTISENSOR APPROACHES

Satellite space-borne remote sensing provides baselines for large-scale lithological mapping [90]. However, new methods are needed for geological applications as a consequence of the limitations of space-borne sensors with respect to their spatial and/or spectral resolution, e.g., LETM+ images consist of eight spectral bands with a spatial resolution of 30 m for bands

1–7 while the panchromatic band 8 has a resolution of 15 m;[1] the hyperspectral environmental mapping and analysis program (EnMAP) [91] has 30 m spatial resolution with more than 240 spectral bands [91]. Within this context, the integration of new Copernicus sensors (both spectral sensors covering the visible to thermal-infrared part of the electromagnetic spectrum and digital elevation data) with higher resolution is of interest in mining and geology communities.

Geological mapping, as well as the detection of potentially economical rock formations, may require high resolutions (both spectral and spatial at the same time) that might not be attained by satellites. To address this issue, airborne and drone-borne data have been used to fill the gap between field and satellite observations.

Drone-borne Laser Scanning (also referred to as LiDAR) supports the structural analysis with information on elevation patterns [92]. UAS hyperspectral data can provide valuable information with respect to narrow absorption features in the visible and near-infrared range (e.g., Rare earth elements or iron-oxides/hydroxides) [93].

Hyperspectral images provide abundant spectral information recorded in several narrow and contiguous bands along the electromagnetic spectrum. However, due to the limited sun irradiance, there is an inevitable tradeoff between spatial and spectral resolutions. Therefore, hyperspectral data with high spectral resolutions usually have low spatial resolutions, which cannot fully identify and delineate the patterns of all the minerals present in the target of interest. On the other hand, the integration of visible images (e.g., RGB or multispectral image) with hyperspectral data provides images with high spatial-spectral resolutions, which produce accurate and more detailed classification results. Furthermore, hyperspectral data in different imaging ranges can record different mineral properties as mentioned in Section II-A. Consequently, many multisensor data fusion approaches have been investigated for more reliable and complete mineral identification in complicated terrain or complex samples, which can be roughly classified into the following two types: pixel-level fusion approaches and feature-level fusion approaches.

A. Pixel-Level Fusion

The pixel-level fusion approaches are used to directly fuse the original images, and then, the fused data are fed into the classifier [94]–[97]. For example, Yokoya *et al.* [94] developed a matrix factorization method for mineral mapping by fusing EnMAP and Sentinel-2 multispectral images, which demonstrated that the spatially enhanced hyperspectral image can contribute to mineral classification. In [95], an intrinsic component decomposition model was used to integrate the RGB and hyperspectral images, where the illumination component was calculated from the RGB image, and the reflectance component was estimated from the hyperspectral image. Here, we briefly describe a recently proposed pixel-level fusion approach, which has been used for mineral mapping.

---

[1][Online]. Available: https://landsat.usgs.gov/what-are-band-designations-landsat-satellites

Let the original image be $\mathbf{X}$. According to the principle of the intrinsic image decomposition model, an ideal hyperspectral image can be modeled as the dot multiplication of the illumination component $\mathbf{S}_H$ and the reflectance component $\mathbf{R}_H$

$$\mathbf{X} = \mathbf{S}_H \cdot \mathbf{R}_H. \tag{13}$$

The aim of this fusion model (13) is to estimate $\mathbf{S}_H$ and $\mathbf{R}_H$ by exploiting a low resolution hyperspectral image and an RGB image. The specific steps are shown as follows:

First, the RGB image is transformed into the YCbCr space, and the luminance band is taken as the estimated illumination component $\mathbf{S}_H$, since the luminance band mainly reflects the spatial details of the RGB image

$$\begin{cases} \mathbf{Y} = 0.257\mathbf{R} + 0.564\mathbf{G} + 0.098\mathbf{B} + 16 \\ \mathbf{Cb} = -0.148\mathbf{R} - 0.291\mathbf{G} + 0.439\mathbf{B} + 128 \\ \mathbf{Cr} = 0.439\mathbf{R} - 0.368\mathbf{G} - 0.071\mathbf{B} + 128 \end{cases} \tag{14}$$

where $\mathbf{Y}$ represents the estimated illumination component $\mathbf{S}_H$.

Then, to estimate the reflectance component, a bicubic downsampling operation with $1/4$ scale is conducted on the original image $\mathbf{X}$ to obtain a low-resolution hyperspectral data $\mathbf{X}_L$. Moreover, the same operation is also conducted on the $\mathbf{S}_H$ to yield a low-resolution illumination component $\mathbf{S}_L$. Based on the principle of intrinsic image decomposition, the low-resolution reflectance component $\mathbf{R}_L$ is calculated by

$$\mathbf{R}_L = \frac{\mathbf{X}_L}{\mathbf{S}_L}. \tag{15}$$

Finally, the fused high-resolution hyperspectral data can be obtained by

$$\mathbf{F} = \mathbf{R}_H \cdot \mathbf{S}_H \tag{16}$$

where $\mathbf{R}_H$ denotes the high-resolution reflectance component, which is obtained by bicubic upsampling ($4\times$ scale).

B. Feature-Level Fusion

The principle of feature-level fusion approaches is to first extract discriminative features from original images, and then, the extracted features are fused together by using a fusion scheme, such as a low-rank model [92], [98], [99], composite kernel [87], [100], and so on [75], [101]. For example, in [26], a sparse and smooth low-rank analysis was developed to integrate multiple optical datasets for mineral classification, where these optical datasets have different spectral and spatial resolutions and different spectral coverage. Ghamisi et al. [87] developed a three-stream CNN for mineral classification, in which a composite kernel technique was used to fuse high-level features obtained by CNN. Here, we describe a general multisensor fusion method called subspace sensor fusion (SubFus) [102], which is presented as follows.

Let original images be $\mathbf{X}_1$ and $\mathbf{X}_2$. First, the morphological profiles (MPs) are used to extract the spatial features of the original images

$$\mathbf{H}_i = \mathrm{MP}(\mathbf{X}_i). \tag{17}$$

Then, the spatial features from different sensors are modeled into a low-dimensional space by using a low-rank representation model

$$(\hat{\mathbf{F}}, \hat{\mathbf{V}}_1, \hat{\mathbf{V}}_2) = \underset{\mathbf{F}, \mathbf{V}_1, \mathbf{V}_2}{\arg\min}\, J(\mathbf{F}, \mathbf{V}_1, \mathbf{V}_2)$$

$$\text{s.t. } \mathbf{V}_1^T \mathbf{V}_1 = \mathbf{I} \text{ and } \mathbf{V}_2^T \mathbf{V}_2 = \mathbf{I} \tag{18}$$

where

$$J(\mathbf{F}, \mathbf{V}_1, \mathbf{V}_2) = \frac{1}{2} \left\| \mathbf{H}_1 - \mathbf{F}\mathbf{V}_1^T \right\|_F^2 + \frac{\lambda_1}{2} \left\| \mathbf{H}_2 - \mathbf{F}\mathbf{V}_2^T \right\|_F^2 + \lambda_2 \mathrm{TV}(\mathbf{F}). \tag{19}$$

Here, λ_1 and λ_2 are the smoothing parameters. The alternating direction method of multipliers [103] is used to solve the objective function (18).

When the fused features are obtained, the spectral classifier is performed on the fused features to yield the classification map.

C. Experimental Results

To assess the classification performance of different fusion methods, pixel-level (i.e., coupled nonnegative matrix factorization (CNMF) [94] and intrinsic image decomposition model-based fusion (IIDF) [95]) and feature-level (SubFus [102]) methods are considered. Experiments are conducted on the Finland dataset.

Fig. 8(e), (g), and (f) presents the classification maps of the fusion methods. The pixel-level fusion method yields noisy classification maps, whereas the feature-level method obtains smoother results. The main reason is that the feature-level fusion method considers the spatial information among neighbor pixels. Furthermore, Table II gives the objective accuracies. By comparing the classification accuracies of SVM, IIDF, and Sub-Fus methods, we can see that the multisensor fusion techniques are able to improve the classification accuracies. Moreover, by comparing the classification accuracies of CNMF, IIDF, and SubFus methods, it is found that the feature-level-based multisensor fusion technique can achieve a better classification performance than those of the pixel-level fusion methods. The reason is that the pixel-level fusion methods enhance the spatial resolution of the original hyperspectral image, whereas the feature-level-based fusion method increases the discrimination of different classes.

V. FROM 2-D RASTER TO 3-D POINT CLOUD

Modern surveying methods, such as light detection and ranging (LiDAR [104]) and structure from motion (see [105]–[107]), directly generate centimeter to sub-centimeter resolution 3-D point clouds. Most workflows convert these to image or raster formats (e.g., digital elevation models or orthomosaics) before further analysis (cf. [105]), but a rapidly increasing number of methods are being developed to work directly with dense point cloud data. Nonetheless, the machine learning tools to process multifeature point clouds do not exist yet.

This approach has several advantages. First, it reduces the total processing required, facilitating the real-time analysis necessary for, e.g., self-driving vehicles and machinery (cf. [108] for a detailed review). Second, it prevents the smoothing and distortion
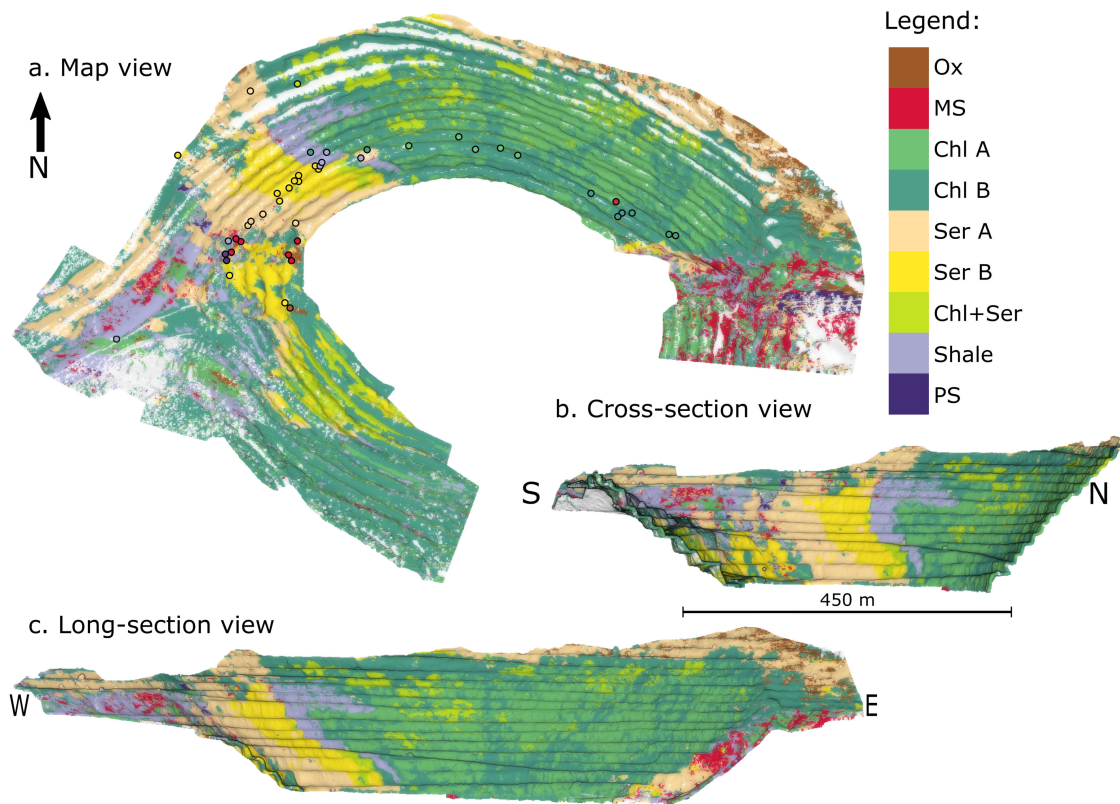
Fig. 9.   Geology map of an open-pit mine in southern Spain (Corta Atalaya, Rio Tinto) created by applying an RF classifier to hypercloud data [116]. The hypercloud approach allowed the fusion of ten ground-based and 357 UAV-based hyperspectral images while simultaneously mitigating distortions and facilitating subsequent 3-D geological interpretation and modeling. Colored circles show the locations, where hand samples were collected and used to train the classifier.

that inevitably occurs when data are projected onto a planar image grid, so retains the original data quality and resolution. Finally, and perhaps most importantly for mapping applications, it allows seamless and true 3-D analysis of arbitrarily complex surfaces.

Open-pit and underground mines tend to have a geometry that severely limits traditional nadir data acquisition and analysis (see Fig. 9). Subvertical pit walls become extremely distorted and spatially unrelated data is juxtaposed by projection to give misleading neighborhood relations or occlusions. While projection onto a different plane (e.g., a cross-section) is suitable in some situations, this is always a compromise, and for many geometries (e.g., tunnels, stopes, and open-pits), no reasonable projection exists [109]. To ameliorate these issues, a small but growing body of research is being conducted in true 3-D using methods specifically developed for point cloud data. These can be divided into the following two distinct but converging categories: 1) spatial methods that make predictions based on geometry and spatial relationships [110]–[115] and 2) spectral methods that use textural features and/or point spectra [116]–[119].

A. State of the Art

Geometric classifiers have become popular in the geotechnical community, where they are frequently used to identify and map subplanar fractures that define rock-faces in mining operations, helping prevent accidents and collapses [110], [111]. Similarly, Weidner *et al.* [112] use a variety of geometric features to distinguish surface materials for geotechnical hazards analysis, while Singh *et al.* [120] use a similar feature set and random sample and consensus algorithm to map geotechnical support (rock bolts) in point clouds of an underground mine captured using a portable laser scanning device. A variety of authors [113]–[115] have also explored the use of dense photogrammetric or LiDAR point clouds to estimate grain size distributions in blasted rock mass, facilitating blast performance analysis and optimization of, e.g., crushing processes. These applications all apply geometric or shallow statistical techniques, so applications of recently developed deep networks (e.g., PointNet; [121]) remain unexplored.

At the other end of the spectrum, geologists are increasingly applying spectral classifiers to remotely sensed point clouds (e.g., hyperclouds; [122]) to map mineralization and associated rock types to optimize mineral extraction or build knowledge that can be used to find new resources. Many of these applications classify each point separately based entirely on its spectral characteristics (e.g., by using the RF method to classify individual point spectra [116]; Fig. 9), but a few approaches that incorporate spatial and texture or reflectance information are beginning to emerge [117]–[119]. These provide a first step toward combined spectral–spatial classification of multi or hyperspectral point clouds.

TABLE III
LIST OF PUBLICLY AVAILABLE SOFTWARE TOOLS FOR PREPROCESSING, SPECIFICALLY DENOISING, AND UNSUPERVISED LEARNING TOOLBOXES

Processing Step	Summary	Resources and Toolboxes
Denoising	Denoising techniques are considered to be an effective solution to reduce existing noise (i.e., instrumental or atmospheric effects) in raw datasets	Noise Reduction in HSI: Overview and Application [30], Image Restoration for Remote Sensing: Overview and Toolbox [130]
Unsupervised learning	Unsupervised (clustering) algorithms cluster the dataset into the meaningful groups	Subspace-based clustering algorithms [55], HESSC [59]
Projection and Correction	Geometric and spectral corrections and conventional spectral analysis techniques (e.g. band ratios, minimum wavelength mapping, linear unmixing)	Hylite [117], MEPHySTo [23], pysptools, spectral python

B. Key Challenges

The main challenges that limit the application of cutting-edge machine learning methods to point cloud data result from the fundamental lack of defined topological structure associated with this data type. This can be an advantage, making, e.g., data fusion relatively straightforward [116], [122], but makes it challenging to define and compute, e.g., neighborhood relationships and gradients. Furthermore, the kernel operations that form the basis of many modern approaches to image classification (e.g., CNNs) cannot be directly translated to unstructured data. Methods based on similar but topologically more flexible approaches are emerging (see [123], [124]), but further work is needed and we are not aware of specific applications in the mining sector yet.

Another more profound challenge relates to the complex dimensionality of point cloud data [125]. Information is recorded in 3-D, but can only be captured from exposed surfaces even though, at least for geological and geotechnical applications, the properties of interest are volumetric. This results in data sampled from an arbitrarily complex manifold embedded in 3-D space, from which volumetric properties need to be interpolated into the subsurface. Current machine learning efforts focus on classifying the surface properties, but there is no fundamental reason they could not also consider and predict volumetric 3-D geometry by combination with advanced geological interpolation techniques (see [126] and [127]).

Finally, point clouds are generally large, so any processing approach inevitably runs into computational challenges that require massive parallelization and out-of-core computation/visualization. Out-of-core visualization methods have advanced significantly, with algorithms like PoTree [128] and EPT[2] able to facilitate visualization of point clouds containing trillions of points (over a standard internet connection[3]). However, out-of-core processing and classification remain a challenge.

VI. LIST OF AVAILABLE RESOURCES

The scientific community has been, fortunately, moving toward open science principles by sharing data, papers, libraries, and software tools. These important principles provide a valuable basis for other researchers to develop their ideas more efficiently, enable reproducible scientific research, and push the boundaries of science forward. In Table III, we share some resources, which could be used by researchers at different stages.

The shared resources in Table III can be summarized as follows.

1) advanced denoising techniques deployed as the final step in preprocessing of datasets used for mineralogical mapping;
2) unsupervised (clustering) algorithms to provide a valuable insight on the under processing datasets without a demand to any prior knowledge; and
3) open-source algorithms for the projection, correction, analyzing hyperspectral data, and fusion of hyperspectral data with 3-D point clouds.

VII. CONCLUDING REMARKS AND FUTURE DIRECTIONS

The field of mining and geology is extremely broad and it is impossible to cover it comprehensively in one literature review. This article focuses particularly on recent advances and algorithmic approaches that have been developed, adapted, or proposed for a particular subject of remote sensing and machine learning for responsible mining, covering a number of key research areas, such as preprocessing, denoising, supervised, and unsupervised classification, multisensor data fusion, and 3-D data interpretation.

The role of remote sensing and machine learning cannot be underestimated for applications related to sustainable mining. Undoubtedly, the use of remote sensing data [both active (e.g., LiDAR) and passive (e.g., hyperspectral)] have been well-established in the geology and mineralogy communities. Machine learning together with remote sensing allow for a systematic investigation of mining applications, providing useful and spatially consistent information in support of evidence-based decision making. The considerable amount of UAVs,

[2][Online]. Available: www.entwine.io
[3][Online]. Available: https://usgs.entwine.io/

airborne, and space-borne data as well as the increasing number of scientific publications on this particular subject demonstrate that the area of remotely sensed data analysis in mining is substantial, dynamic, and vibrant.

The collection of adequate high-quality ground truth is one of the most challenging issues in developing scalable machine learning approaches for mining-related applications. These are needed both for training data-hungry DL approaches and for evaluating their outputs, but are costly and time-consuming to develop. For geological applications, these challenges are compounded by a philosophical issue: All geology maps are interpretations, often with a specific context, framing or goal, so it is very difficult to define "ground-truth" labels in a rigorous and meaningful way [130], [131].

One possible means for ameliorating this issue is to instead focus on estimating mineral abundance, as this can be robustly (albeit expensively) quantified. Standard and widely applied geological classification schemes could then be applied to translate mineralogy into geological labels (e.g., [132]). This approach also opens the possibility of using spectral libraries containing measurements for minerals and mineral mixtures as training data (e.g., [133]–[137]). But, as discussed by Thiele *et al.* [116], translating between laboratory data and remotely sensed spectra is fraught with additional challenges. Despite these challenges, carefully designed approaches can derive significant value from spectral library datasets (e.g., [138], [139]).

The general lack of training and validation data should also be tackled in the following two complementary ways: 1) From the theoretical point of view, more emphasis should be dedicated to the development of unsupervised, weak-supervised, or self-supervised approaches to produce classification and change maps partially independent from the existence of high-quality and high-amount of labeled data. 2) It is important to move away from closed data to more open science principles by making data, software tools, and libraries publicly available. These developments push this vibrant community forward and will eventually lead to transparent and reproducible scientific research, reuseable data and methods, and more efficient creation of new data products.

From the methodological perspective, several research directions still demand developments. First of all, with the great opportunity of acquiring multimodal datasets, developing multisensor and multiscale fusion algorithms are vital and of great demand since such approaches enable us to benefit from enriched datasets from different sources. Second, as mentioned before, it is expensive and time-consuming to annotate a large number of training sets for mineral mapping. Therefore, the development of advanced classification approaches that are able to produce accurate maps using scarce limited samples is of vital importance. Furthermore, captured multisensor data are usually contaminated with different noise types. How to improve the quality of the input data shapes an important line of research. The success of this step can largely influence the success of the further processing steps, such as mapping and tracking.

The future mine will require series of imaging sensors that will acquire continuous data streams from multiple platforms.

Data will be required to process in real-time to allow rapid decision-making and process adaptation. This review highlights the bottlenecks, challenges but also the immense progress made by the community toward these goals.

REFERENCES

[1] F. Krausmann, C. Lauk, W. Haas, and D. Wiedenhofer, "From resource extraction to outflows of wastes and emissions: The socioeconomic metabolism of the global economy, 1900–2015," *Glob. Environ. Change*, vol. 52, pp. 131–140, 2018.

[2] European Commission, "Study on the EU's list of critical raw materials—Final Report," Eur. Commission, Brussels, Belgium, Rep., 2020.

[3] Canadian Government, "Canadian critical minerals list," Accessed: Mar. 15, 2021. [Online]. Available: https://www.nrcan.gc.ca/criticalminerals

[4] M. Kesselring, F. Wagner, M. Kirsch, L. Ajjabou, and R. Gloaguen, "Sustainable test sites for mineral exploration: Development of sustainable test sites and knowledge spillover for industry," *Sustainability*, vol. 12, no. 5, 2020, Art. no. 2016.

[5] O. Renn, G. Beier, and P.-J. Schweizer, "The opportunities and risks of digitalisation for sustainable development: A systemic perspective," *GAIA-Ecological Perspectives Sci. Soc.*, vol. 30, no. 1, pp. 23–28, 2021.

[6] C. Sonesson, G. Davidson, L. Sachs, Columbia Center on Sustainable Investment (CCSI), UNDP, UN Sustainable Development Solutions Network (SDSN), and World Economic Forum, "Mapping mining to the sustainable development goals: An Atlas," Sustainable Development Solutions Network, White Paper, p. 2, Accessed: Sep. 10, 2021. [Online]. Available: http://www.jstor.org/stable/resrep15880.3

[7] R. Booysen, "The potential of drones in multi-scale hyperspectral imaging for mineral exploration: Examples from Southern Africa," Ph.D. dissertation, School Geosci., Univ. Witwatersrand, Johannesburg, South Africa, Apr. 2021.

[8] J. Lööw, L. Abrahamsson, and J. Johansson, "Mining 4.0-the impact of new technology from a work place perspective," *Mining, Metall. Exploration*, vol. 36, no. 4, pp. 701–707, 2019.

[9] B. Hubbard, J. Crowley, and D. Zimbelman, "Comparative alteration mineral mapping using visible to shortwave infrared (0.4–2.4 μm) hyperion, ALI, and ASTER imagery," *IEEE Trans. Geosci. Remote Sens.*, vol. 41, no. 6, pp. 1401–1410, Jul. 2003.

[10] R. Richter and D. Schläpfer, "Atmospheric/topographic correction for satellite imagery," German Aerosp. Center, Wessling, Germany, Rep. LR-IB 565-02/11, 2011.

[11] T. Cooley *et al.*, "FLAASH, a MODTRAN4-based atmospheric correction algorithm, its application and validation," in *Proc. IEEE Int. Geosci. Remote Sens. Symp.*, 2002, pp. 1414–1418.

[12] S. van der Linden *et al.*, "The EnMAP-box-A toolbox and application programming interface for EnMAP data processing," *Remote Sens.*, vol. 7, no. 9, pp. 11249–11266, 2015.

[13] J. Feng, D. Rogge, and B. Rivard, "Comparison of lithological mapping results from airborne hyperspectral VNIR-SWIR, LWIR and combined data," *Int. J. Appl. Earth Observ. Geoinf.*, vol. 64, pp. 340–353, 2018.

[14] L. C. Rowan, T. L. Bowers, J. K. Crowley, C. Anton-Pacheco, P. Gumiel, and M. J. Kingston, "Analysis of airborne visible-infrared imaging spectrometer (AVIRIS) data of the Iron Hill, Colorado, carbonatite-alkalic igneous complex," *Econ. Geol.*, vol. 90, no. 7, pp. 1966–1982, 1995.

[15] A. A. Zhilenkov and I. R. Epifantsev, "System of autonomous navigation of the drone in difficult conditions of the forest trails," in *Proc. IEEE Conf. Russian Young Researchers Elect. Electron. Eng.*, 2018, pp. 1036–1039.

[16] A. Santangeli, Y. Chen, E. Kluen, R. Chirumamilla, J. Tiainen, and J. Loehr, "Integrating drone-borne thermal imaging with artificial intelligence to locate bird nests on agricultural land," *Sci. Rep.*, vol. 10, no. 1, 2020, Art. no. 10993.

[17] S. Jakob, R. Zimmermann, and R. Gloaguen, "The need for accurate geometric and radiometric corrections of drone-borne hyperspectral data for mineral exploration: MEPHySTo—A toolbox for pre-processing drone-borne hyperspectral data," *Remote Sens.*, vol. 9, 2017, Art. no. 88.

[18] O. Nevalainen *et al.*, "Individual tree detection and classification with UAV-based photogrammetric point clouds and hyperspectral imaging," *Remote Sens.*, vol. 9, no. 3, 2017, Art. no. 185.

[19] E. Yanmaz, S. Yahyanejad, B. Rinner, H. Hellwagner, and C. Bettstetter, "Drone networks: Communications, coordination, and sensing," *Ad Hoc Netw.*, vol. 68, pp. 1–15, 2018.

[20] R. N. Greenberger, B. L. Ehlmann, P. W. Jewell, L. P. Birgenheier, and R. O. Green, "Detection of organic-rich oil shales of the Green river formation, Utah, with ground-based imaging spectroscopy," in *Proc. 8th Workshop Hyperspectral Image Signal Process. Evol. Remote Sens.*, 2016, pp. 1–5.

[21] L. Sun, S. D. Khan, S. Sarmiento, M. Lakshmikantha, and H. Zhou, "Ground-based hyperspectral imaging and terrestrial laser scanning for fracture characterization in the Mississippian Boone Formation," *Int. J. Appl. Earth Observ. Geoinf.*, vol. 63, pp. 222–233, 2017.

[22] S. Boubanga-Tombet *et al.*, "Thermal infrared hyperspectral imaging for mineralogy mapping of a mine face," *Remote Sens.*, vol. 10, no. 10, 2018, Art. no. 1518.

[23] S. Lorenz, "The need for accurate pre-processing and data integration for the application of hyperspectral imaging in mineral exploration," Ph.D. dissertation, Faculty Geoscie., Geotech. Min., TU Bergakademie Freiberg, Freiberg, Germany, Oct. 2019.

[24] J. R. Jensen, *Remote Sensing of the Environment: An Earth Resource Perspective*, 2nd ed. Englewood Cliffs, NJ, USA: Prentice-Hall, 2009.

[25] S. Thiele, S. Lorenz, M. Kirsch, and R. Gloaguen, "A novel and open-source illumination correction for hyperspectral digital out-crop models," *IEEE Trans. Geosci. Remote Sens.*, to be published, doi: 10.1109/TGRS.2021.3098725.

[26] B. Rasti, P. Ghamisi, P. Seidel, S. Lorenz, and R. Gloaguen, "Multiple optical sensor fusion for mineral mapping of core samples," *Sensors*, vol. 20, no. 13, 2020, Art. no. 3766.

[27] M. Mitchley, M. Sears, and S. Damelin, "Target detection in hyperspectral mineral data using wavelet analysis," in *Proc. IEEE Int. Geosci. Remote Sens. Symp.*, 2009, pp. IV-881–IV-884.

[28] B. Rasti, B. Koirala, P. Scheunders, and P. Ghamisi, "How hyperspectral image unmixing and denoising can boost each other," *Remote Sens.*, vol. 12, no. 11, May 2020, Art. no. 1728.

[29] F. Lin, K. Chen, X. Wang, H. Cao, D. Chen, and F. Chen, "Denoising stacked autoencoders for transient electromagnetic signal denoising," *Nonlinear Processes Geophys.*, vol. 26, no. 1, pp. 13–23, 2019.

[30] B. Rasti, P. Scheunders, P. Ghamisi, G. Licciardi, and J. Chanussot, "Noise reduction in hyperspectral imagery: Overview and application," *Remote Sens.*, vol. 10, no. 3, 2018, Art. no. 482.

[31] N. Acito, M. Diani, and G. Corsini, "Subspace-based striping noise reduction in hyperspectral images," *IEEE Trans. Geosci. Remote Sens.*, vol. 49, no. 4, pp. 1325–1342, Apr. 2011.

[32] M. D. Bisceglie, R. Episcopo, C. Galdi, and S. L. Ullo, "Destriping MODIs data using overlapping field-of-view method," *IEEE Trans. Geosci. Remote Sens.*, vol. 47, no. 2, pp. 637–651, Feb. 2009.

[33] D. Donoho and I. M. Johnstone, "Adapting to unknown smoothness via wavelet shrinkage," *J. Amer. Statist. Assoc.*, vol. 90, pp. 1200–1224, 1995.

[34] M. Elad, *Sparse and Redundant Representations: From Theory to Applications in Signal and Image Processing*, 1st ed. Berlin, Germany: Springer, 2010.

[35] B. Rasti, J. R. Sveinsson, M. O. Ulfarsson, and J. A. Benediktsson, "Hyperspectral image denoising using 3D wavelets," in *Proc. IEEE Int. Geosci. Remote Sens. Symp.*, 2012, pp. 1349–1352.

[36] B. Rasti, "Sparse hyperspectral image modeling and restoration," Ph.D. dissertation, Dept. Elect. Comput. Eng., Univ. Iceland, Reykjavik, Iceland, Dec. 2014.

[37] V. Chandrasekaran, S. Sanghavi, P. A. Parrilo, and A. S. Willsky, "Sparse and low-rank matrix decompositions," *IFAC Proc. Volumes.*, vol. 42, no. 10, pp. 1493–1498, 2009.

[38] E. J. Candès, X. Li, Y. Ma, and J. Wright, "Robust principal component analysis?," *J. ACM*, vol. 58, no. 3, pp 1-37, Jun. 2011.

[39] B. Rasti, J. R. Sveinsson, M. O. Ulfarsson, and J. A. Benediktsson, "A new linear model and sparse regularization," in *Proc. IEEE Int. Geosci. Remote Sens. Symp.*, Jul. 2013, pp. 457–460.

[40] H. Zhang, W. He, L. Zhang, H. Shen, and Q. Yuan, "Hyperspectral image restoration using low-rank matrix recovery," *IEEE Trans. Geosci. Remote Sens.*, vol. 52, no. 8, pp. 4729–4743, Aug. 2014.

[41] B. Rasti, M. O. Ulfarsson, and P. Ghamisi, "Automatic hyperspectral image restoration using sparse and low-rank modeling," *IEEE Geosci. Remote Sens. Lett.*, vol. 14, no. 12, pp. 2335–2339, Dec. 2017.

[42] B. Rasti, M. O. Ulfarsson, and J. R. Sveinsson, "Hyperspectral subspace identification using SURE," *IEEE Geosci. Remote Sens. Lett.*, vol. 12, no. 12, pp. 2481–2485, Dec. 2015.

[43] L. Zhuang and J. M. Bioucas-Dias, "Fast hyperspectral image denoising and inpainting based on low-rank and sparse representations," *IEEE J. Sel. Topics Appl. Earth Observ. Remote Sens.*, vol. 11, no. 3, pp. 730–742, Mar. 2018.

[44] K. Dabov, A. Foi, V. Katkovnik, and K. Egiazarian, "Image denoising by sparse 3-D transform-domain collaborative filtering," *IEEE Trans. Image Process.*, vol. 16, no. 8, pp. 2080–2095, Aug. 2017.

[45] W. He, H. Zhang, L. Zhang, and H. Shen, "Hyperspectral image denoising via noise-adjusted iterative low-rank matrix approximation," *IEEE J. Sel. Topics. Appl. Earth Observ. Remote Sens.*, vol. 8, no. 6, pp. 3050–3061, Jun. 2015.

[46] L. Gao, D. Yao, Q. Li, L. Zhuang, B. Zhang, and J. M. Bioucas-Dias, "A new low-rank representation based hyperspectral image denoising method for mineral mapping," *Remote Sens.*, vol. 9, no. 11, 2017, Art. no. 1145.

[47] L. I. Rudin, S. Osher, and E. Fatemi, "Nonlinear total variation based noise removal algorithms," *Phys. D Nonlinear Phenomena*, vol. 60, no. 1–4, pp. 259–268, Nov. 1992.

[48] H. K. Aggarwal and A. Majumdar, "Hyperspectral image denoising using spatio-spectral total variation," *IEEE Geosci. Remote Sens. Lett.*, vol. 13, no. 3, pp. 442–446, Mar. 2016.

[49] B. Rasti, P. Ghamisi, and J. A. Benediktsson, "Hyperspectral mixed Gaussian and sparse noise reduction," *IEEE Geosci. Remote Sens. Lett.*, vol. 17, no. 3, pp. 474–478, Mar. 2020.

[50] B. Rasti, J. R. Sveinsson, and M. O. Ulfarsson, "Total variation based hyperspectral feature extraction," in *Proc. IEEE Int. Geosci. Remote Sens. Symp.*, 2014, pp. 4644–4647.

[51] D. Ulyanov, A. Vedaldi, and V. Lempitsky, "Deep image prior," *Int. J. Comput. Vis.*, vol. 128, no. 7, pp. 1867–1888, Mar. 2020.

[52] J. Lehtinen *et al.*, "Noise2Noise: Learning image restoration without clean data," in *Proc. 35th Int. Conf. Mach. Learn., Proc. Mach. Learn. Res.*, Jul. 2018, vol. 80, pp. 2965–2974.

[53] P. Ghamisi *et al.*, "Advances in hyperspectral image and signal processing: A comprehensive overview of the state of the art," *IEEE Geosci. Remote Sens. Mag.*, vol. 5, no. 4, pp. 37–78, Dec. 2017.

[54] B. Rasti *et al.*, "Feature extraction for hyperspectral imagery: The evolution from shallow to deep: Overview and toolbox," *IEEE Geosci. Remote Sens. Mag.*, vol. 8, no. 4, pp. 60–88, Dec. 2020.

[55] C. You, C. Li, D. Robinson, and R. Vidal, "Self-representation based unsupervised exemplar selection in a union of subspaces," *IEEE Trans. Pattern Anal. Mach. Intell.*, to be published, doi: 10.1109/TPAMI.2020.3035599.

[56] H. Zhai, H. Zhang, L. Pingxiang, and L. Zhang, "Hyperspectral image clustering: Current achievements and future lines," *IEEE Geosci. Remote Sens. Mag.*, to be published, doi: 10.1109/MGRS.2020.3032575.

[57] H. Zhang, H. Zhai, L. Zhang, and P. Li, "Spectral-spatial sparse subspace clustering for hyperspectral remote sensing images," *IEEE Trans. Geosci. Remote Sens.*, vol. 54, no. 6, pp. 3672–3684, Jun. 2016.

[58] E. Elhamifar and R. Vidal, "Sparse subspace clustering: Algorithm, theory, and applications," *IEEE Trans. Pattern Anal. Mach. Intell.*, vol. 35, no. 11, pp. 2765–2781, Nov. 2013.

[59] K. R. Shahi, M. Khodadadzadeh, L. Tusa, P. Ghamisi, R. Tolosana-Delgado, and R. Gloaguen, "Hierarchical sparse subspace clustering (HESSC): An automatic approach for hyperspectral image analysis," *Remote Sens.*, vol. 12, no. 15, 2020, Art. no. 2421.

[60] D. Lavenier, *FPGA Implementation of the k-Means Clustering Algorithm for Hyperspectral Images*, Los Alamos National Laboratory, Los Alamos, NM, USA, 2000.

[61] R. Vidal, "Subspace clustering," *IEEE Signal Process. Mag.*, vol. 28, no. 2, pp. 52–68, Mar. 2011.

[62] C. You, D. Robinson, and R. Vidal, "Scalable sparse subspace clustering by orthogonal matching pursuit," in *Proc. IEEE Conf. Comput. Vis. Pattern Recognit.*, 2016, pp. 3918–3927.

[63] E. Min, X. Guo, Q. Liu, G. Zhang, J. Cui, and J. Long, "A survey of clustering with deep learning: From the perspective of network architecture," *IEEE Access*, vol. 6, pp. 39 501–39514, 2018.

[64] Y. Guo, J. Gao, and F. Li, "Spatial subspace clustering for drill hole spectral data," *J. Appl. Remote Sens.*, vol. 8, no. 1, pp. 1–20, 2014.

[65] F. Fouedjio, E. J. Hill, and C. Laukamp, "Geostatistical clustering as an aid for ore body domaining: Case study at the Rocklea Dome channel iron ore deposit, Western Australia," *Appl. Earth Sci.*, vol. 127, no. 1, pp. 15–29, 2018.

[66] K. R. Shahi, M. Khodadadzadeh, R. Tolosana-delgado, L. Tusa, and R. Gloaguen, "The application of subspace clustering algorithms in drill-core hyperspectral domaining," in *Proc. 10th Workshop Hyperspectral Imag. Signal Process. Evol. Remote Sens.*, 2019, pp. 1–5.

[67] K. R. Shahi, P. Ghamisi, B. Rasti, R. Jackisch, P. Scheunders, and R. Gloaguen, "Data fusion using a multi-sensor sparse-based clustering algorithm," *Remote Sens.*, vol. 12, no. 23, 2020, Art. no. 4007.

[68] K. R. Shahi, P. Ghamisi, R. Jackisch, B. Rasti, P. Scheunders, and R. Gloaguen, "A multi-sensor subspace-based clustering algorithm using RGB and hyperspectral data," in *Proc. 11th Workshop Hyperspectral Imag. Signal Process. Evol. Remote Sens.*, 2021, pp. 1–5.

[69] J. C. Bezdek, *Pattern Recognition With Fuzzy Objective Function Algorithms*. Berlin, Germany: Springer, 2013.

[70] D. Cai and X. Chen, "Large scale spectral clustering via landmark-based sparse representation," *IEEE Trans. Cybern.*, vol. 45, no. 8, pp. 1669–1680, Aug. 2015.

[71] S. Li, W. Song, L. Fang, Y. Chen, P. Ghamisi, and J. A. Benediktsson, "Deep learning for hyperspectral image classification: An overview," *IEEE Trans. Geosci. Remote Sens.*, vol. 57, no. 9, pp. 6690–6709, Sep. 2019.

[72] D. R. N. Clark, "USGS digital spectral library," Sep. 2007. [Online]. Available: http://speclab.cr.usgs.gov/spectral-lib.html

[73] E. F. Littlefield and W. M. Calvin, "Geothermal exploration using imaging spectrometer data over Fish Lake Valley, Nevada," *Remote Sens. Environ.*, vol. 140, pp. 509–518, 2014.

[74] W. M. Calvin and E. L. Pace, "Mapping alteration in geothermal drill core using a field portable spectroradiometer," *Geothermics*, vol. 61, pp. 12–23, 2016.

[75] I. C. C. Acosta, M. Khodadadzadeh, L. Tusa, P. Ghamisi, and R. Gloaguen, "A machine learning framework for drill-core mineral mapping using hyperspectral and high-resolution mineralogical data fusion," *IEEE J. Sel. Topics Appl. Earth Observ. Remote Sens.*, vol. 12, no. 12, pp. 4829–4842, Dec. 2019.

[76] I. C. C. Acosta, M. Khodadadzadeh, R. Tolosana-Delgado, and R. Gloaguen, "Drill-core hyperspectral and geochemical data integration in a superpixel-based machine learning framework," *IEEE J. Sel. Topics Appl. Earth Observ. Remote Sens.*, vol. 13, no. 1, pp. 4214–4228, Jul. 2020.

[77] P. Ghamisi, J. Plaza, Y. Chen, J. Li, and A. J. Plaza, "Advanced spectral classifiers for hyperspectral images: A review," *IEEE Geosci. Remote Sens. Mag.*, vol. 5, no. 1, pp. 8–32, Mar. 2017.

[78] P. Duan, X. Kang, S. Li, P. Ghamisi, and J. A. Benediktsson, "Fusion of multiple edge-preserving operations for hyperspectral image classification," *IEEE Trans. Geosci. Remote Sens.*, vol. 57, no. 12, pp. 10 336–10 349, Dec. 2019.

[79] J. Xia, P. Ghamisi, N. Yokoya, and A. Iwasaki, "Random forest ensembles and extended multiextinction profiles for hyperspectral image classification," *IEEE Trans. Geosci. Remote Sens.*, vol. 56, no. 1, pp. 202–216, Jan. 2018.

[80] J. Li, J. M. Bioucas-Dias, and A. Plaza, "Spectral-spatial hyperspectral image segmentation using subspace multinomial logistic regression and Markov random fields," *IEEE Trans. Geosci. Remote Sens.*, vol. 50, no. 3, pp. 809–823, Mar. 2012.

[81] C. J. Burges, "A tutorial on support vector machines for pattern recognition," *Data Mining Knowl. Discov.*, vol. 56, no. 1, pp. 202–216, Jun. 2018.

[82] S. Lorenz, P. Ghamisi, M. Kirsch, R. Jackisch, B. Rasti, and R. Gloaguen, "Feature extraction for hyperspectral mineral domain mapping: A test of conventional and innovative methods," *Remote Sens. Environ.*, vol. 252, 2021, Art. no. 112129.

[83] S. Prasad and L. M. Bruce, "Limitations of principal components analysis for hyperspectral target recognition," *IEEE Geosci. Remote Sens. Lett.*, vol. 5, no. 4, pp. 625–629, Oct. 2008.

[84] A. A. Green, M. Berman, P. Switzer, and M. D. Craig, "A transformation for ordering multispectral data in terms of image quality with implications for noise removal," *IEEE Trans. Geosci. Remote Sens.*, vol. 26, no. 1, pp. 65–74, Jan. 1988.

[85] B. Rasti, M. O. Ulfarsson, and J. R. Sveinsson, "Hyperspectral feature extraction using total variation component analysis," *IEEE Trans. Geosci. Remote Sens.*, vol. 54, no. 12, pp. 6976–6985, Dec. 2016.

[86] B. Rasti, J. R. Sveinsson, and M. O. Ulfarsson, "Wavelet-based sparse reduced-rank regression for hyperspectral image restoration," *IEEE Trans. Geosci. Remote Sens.*, vol. 52, no. 10, pp. 6688–6698, Oct. 2014.

[87] P. Ghamisi, H. Li, R. Jackisch, B. Rasti, and R. Gloaguen, "Remote sensing and deep learning for sustainable mining," in *Proc. IEEE Int. Geosci. Remote Sens. Symp.*, 2020, pp. 3739–3742.

[88] F. Melgani and L. Bruzzone, "Classification of hyperspectral remote sensing images with support vector machines," *IEEE Trans. Geosci. Remote Sens.*, vol. 42, no. 8, pp. 1778–1790, Aug. 2004.

[89] P. Duan, P. Ghamisi, X. Kang, B. Rasti, S. Li, and R. Gloaguen, "Fusion of dual spatial information for hyperspectral image classification," *IEEE Trans. Geosci. Remote Sens.*, vol. 59, no. 9, pp. 7726–7738, Sep. 2021.

[90] R. Gloaguen *et al.*, "Multi-source and multi-scale imaging-data integration to boost mineral mapping," in *Proc. IEEE Int. Geosci. Remote Sens. Symp.*, 2019, pp. 5587–5589.

[91] H. Kaufmann *et al.*, "EnMAP A hyperspectral sensor for environmental mapping and analysis," in *Proc. IEEE Int. Symp. Geosci. Remote Sens.*, 2006, pp. 1617–1619.

[92] P. Duan, X. Kang, P. Ghamisi, and Y. Liu, "Multilevel structure extraction-based multi-sensor data fusion," *Remote Sens.*, vol. 12, no. 24, 2020, Art. no. 4034.

[93] H. Flores *et al.*, "UAS-based hyperspectral environmental monitoring of acid mine drainage affected waters," *Minerals*, vol. 11, no. 2, 2021, Art. no. 182.

[94] N. Yokoya, J. C.-W. Chan, and K. Segl, "Potential of resolution-enhanced hyperspectral data for mineral mapping using simulated enmap and sentinel-2 images," *Remote Sens.*, vol. 8, no. 3, 2016, Art. no. 172.

[95] P. Duan *et al.*, "Component decomposition-based hyperspectral resolution enhancement for mineral mapping," *Remote Sens.*, vol. 12, no. 18, 2020, Art. no. 2903.

[96] F. A. Kruse and S. L. Perry, "Regional mineral mapping by extending hyperspectral signatures using multispectral data," in *Proc. IEEE Aerosp. Conf.*, 2007, pp. 1–14.

[97] L. Ni, H. Xu, and X. Zhou, "Mineral identification and mapping by synthesis of hyperspectral VNIR/SWIR and multispectral TIR remotely sensed data with different classifiers," *IEEE J. Sel. Topics Appl. Earth Observ. Remote Sens.*, vol. 13, no. 1, pp. 3155–3163, Jun. 2020.

[98] B. Rasti, P. Ghamisi, J. Plaza, and A. Plaza, "Fusion of hyperspectral and LiDAR data using sparse and low-rank component analysis," *IEEE Trans. Geosci. Remote Sens.*, vol. 55, no. 11, pp. 6354–6365, Nov. 2017.

[99] B. Rasti, P. Ghamisi, and R. Gloaguen, "Hyperspectral and LiDAR fusion using extinction profiles and total variation component analysis," *IEEE Trans. Geosci. Remote Sens.*, vol. 55, no. 7, pp. 3997–4007, Jul. 2017.

[100] P. Ghamisi, B. Rasti, and J. A. Benediktsson, "Multisensor composite Kernels based on extreme learning machines," *IEEE Geosci. Remote Sens. Lett.*, vol. 16, no. 2, pp. 196–200, Feb. 2019.

[101] S. Lorenz *et al.*, "Multi-sensor spectral imaging of geological samples: A data fusion approach using spatio-spectral feature extraction," *Sensors*, vol. 19, no. 12, 2019, Art. no. 2787.

[102] B. Rasti and P. Ghamisi, "Remote sensing image classification using subspace sensor fusion," *Inf. Fusion*, vol. 64, pp. 121–130, 2020.

[103] J. Eckstein and D. P. Bertsekas, "On the Douglas-Rachford splitting method and the proximal point algorithm for maximal monotone operators," *Math. Program.*, vol. 55, pp. 293–318, 1992.

[104] S. J. Buckley, J. A. Howell, H. D. Enge, and T. H. Kurz, "Terrestrial laser scanning in geology: Data acquisition, processing and accuracy considerations," *J. Geological Soc.*, vol. 165, no. 3, pp. 625–638, 2008.

[105] S. Park and Y. Choi, "Applications of unmanned aerial vehicles in mining from exploration to reclamation: A review," *Minerals*, vol. 10, no. 8, 2020, Art. no. 663.

[106] D. D. Tannant, "Review of photogrammetry-based techniques for characterization and hazard assessment of rock faces," *Int. J. Georesour. Environ.*, vol. 1, no. 2, pp. 76–87, 2015.

[107] S. P. Bemis *et al.*, "Ground-based and UAV-based photogrammetry: A multi-scale, high-resolution mapping tool for structural geology and paleoseismology," *J. Struct. Geol.*, vol. 69, pp. 163–178, 2014.

[108] D. Fernandes *et al.*, "Point-cloud based 3D object detection and classification methods for self-driving applications: A survey and taxonomy," *Inf. Fusion*, vol. 68, pp. 161–191, 2021.

[109] S. T. Thiele, L. Grose, A. Samsu, S. Micklethwaite, S. A. Vollgger, and A. R. Cruden, "Rapid, semi-automatic fracture and contact mapping for point clouds, images and geophysical data," *Solid Earth*, vol. 8, no. 6, pp. 1241–1253, 2017.

[110] D. García-Sellés, O. Falivene, P. Arbués, O. Gratacos, S. Tavani, and J. A. Muñoz, "Supervised identification and reconstruction of near-planar geological surfaces from terrestrial laser scanning," *Comput. Geosci.*, vol. 37, no. 10, pp. 1584–1594, Oct. 2011.

[111] S. Slob, B. Van Knapen, R. Hack, K. Turner, and J. Kemeny, "Method for automated discontinuity analysis of rock slopes with three-dimensional laser scanning," *Transp. Res. Rec.*, vol. 1913, no. 1, pp. 187–194, 2005.

[112] L. Weidner, G. Walton, and R. Kromer, "Classification methods for point clouds in rock slope monitoring: A novel machine learning approach and comparative analysis," *Eng. Geol.*, vol. 263, Dec. 2019, Art. no. 105326.

[113] D. A. Bonneau and D. J. Hutchinson, "The use of multi-scale dimensionality analysis for the characterization of debris distribution patterns," in *Proc. Geohazards 7-Eng. Resilence Changing Climate*, 2018, pp. 748–759.

[114] I. C. Engin, "Comparison of the different mathematical methods performed in determining the size distribution of aggregates using LiDAR point cloud data and suggested algorithm," *Earth Sci. Informat.*, vol. 12, no. 3, pp. 365–380, Sep. 2019.

[115] H. Jang *et al.*, "Development of 3D rock fragmentation measurement system using photogrammetry," *Int. J. Mining, Reclamation Environ.*, vol. 34, no. 4, pp. 294–305, Apr. 2020.

[116] S. Thiele *et al.*, "Multi-scale, multi-sensor data integration for automated 3-D geological mapping using hylite," *Ore Geol. Rev.*, vol. 136, 2021, Art. no. 104252.

[117] F. Beretta, A. L. Rodrigues, R. L. Peroni, and J. Costa, "Automated lithological classification using UAV and machine learning on an open cast mine," *Appl. Earth Sci.*, vol. 128, no. 3, pp. 79–88, 2019.

[118] J. Guo *et al.*, "A geometry- and texture-based automatic discontinuity trace extraction method for rock mass point cloud," *Int. J. Rock Mech. Mining Sci.*, vol. 124, Dec. 2019, Art. no. 104132.

[119] G. Walton, G. Mills, G. Fotopoulos, R. Radovanovic, and R. Stancliffe, "An approach for automated lithological classification of point clouds," *Geosphere*, vol. 12, no. 6, pp. 1833–1841, Dec. 2016.

[120] S. K. Singh, S. Raval, and B. Banerjee, "A robust approach to identify roof bolts in 3D point cloud data captured from a mobile laser scanner," *Int. J. Mining Sci. Technol.*, vol. 31, no. 2, pp. 303–312, Mar. 2021.

[121] C. R. Qi, H. Su, K. Mo, and L. J. Guibas, "PointNet: Deep learning on point sets for 3D classification and segmentation," in *Proc. IEEE Conf. Comput. Vis. Pattern Recognit.*, 2017, pp. 652–660.

[122] S. Lorenz *et al.*, "Radiometric correction and 3D integration of long-range ground-based hyperspectral imagery for mineral exploration of vertical outcrops," *Remote Sens.*, vol. 10, no. 2, Feb. 2018, Art. no. 176.

[123] G. Li, M. Muller, A. Thabet, and B. Ghanem, "DeepGCNs: Can GCNs go as deep as CNNs?," in *Proc. IEEE/CVF Int. Conf. Comput. Vis.*, 2019, pp. 9267–9276.

[124] J. Zhang, X. Hu, and H. Dai, "A graph-voxel joint convolution neural network for ALS point cloud segmentation," *IEEE Access*, vol. 8, pp. 139781–139791, 2020.

[125] N. Brodu and D. Lague, "3D terrestrial lidar data classification of complex natural scenes using a multi-scale dimensionality criterion: Applications in geomorphology," *ISPRS J. Photogrammetry Remote Sens.*, vol. 68, pp. 121–134, Mar. 2012.

[126] L. Grose, L. Ailleres, G. Laurent, and M. Jessell, "LoopStructural 1.0: Time aware geological modelling," *Geosci. Model Develop.*, vol. 14, no. 6, pp. 3915–39372021.

[127] M. d. l. Varga, A. Schaaf, and F. Wellmann, "GemPy 1.0: Open-source stochastic geological modeling and inversion," *Geosci. Model Develop.*, vol. 12, no. 1, pp. 1–32, 2019.

[128] M. Schütz, S. Ohrhallinger, and M. Wimmer, "Fast out-of-core octree generation for massive point clouds," *Comput. Graph. Forum*, vol. 39, no. 7, pp. 155–167, 2020.

[129] B. Rasti, Y. Chang, E. Dalsasso, L. Denis, and P. Ghamisi, "Image restoration for remote sensing: Overview and toolbox," 2021, *arXiv:2107.00557*.

[130] R. Frodeman, "Geological reasoning: Geology as an interpretive and historical science," *Geol. Soc. Amer. Bull.*, vol. 107, no. 8, pp. 960–968, 1995.

[131] C. E. Bond, "Uncertainty in structural interpretation: Lessons to be learnt," *J. Struct. Geol.*, vol. 74, pp. 185–200, 2015.

[132] M. L. Bas and A. L. Streckeisen, "The IUGS systematics of igneous rocks," *J. Geol. Soc.*, vol. 148, no. 5, pp. 825–833, 1991.

[133] R. F. Kokaly *et al.*, "USGS spectral library version 7," U.S. Geol. Surv., Reston, VA, USA, Tech. Rep., 2017.

[134] R. V. Rossel *et al.*, "A global spectral library to characterize the world's soil," *Earth-Sci. Rev.*, vol. 155, pp. 198–230, 2016.

[135] M. Schodlok, A. Green, and J. Huntington, "A reference library of thermal infrared mineral reflectance spectra for the HyLogger-3 Drill core logging system," *Australian J. Earth Sci.*, vol. 63, no. 8, pp. 941–949, 2016.

[136] P. R. Christensen *et al.*, "A thermal emission spectral library of rock-forming minerals," *J. Geophys. Res., Planets*, vol. 105, no. E4, pp. 9735–9739, 2000.

[137] A. M. Baldridge, S. Hook, C. Grove, and G. Rivera, "The ASTER spectral library version 2.0," *Remote Sens. Environ.*, vol. 113, no. 4, pp. 711–715, 2009.

[138] G. A. Swayze *et al.*, "Mapping advanced argillic alteration at Cuprite, Nevada, using imaging spectroscopy," *Econ. Geol.*, vol. 109, no. 5, pp. 1179–1221, 2014.

[139] L. Sun, F. Wu, T. Zhan, W. Liu, J. Wang, and B. Jeon, "Weighted nonlocal low-rank tensor decomposition method for sparse unmixing of hyperspectral images," *IEEE J. Sel. Topics Appl. Earth Observ. Remote Sens.*, vol. 13, no. 1, pp. 1174–1188, 2020.